PCCP

PAPER

View Article Online
View Journal | View Issue

Cite this: *Phys. Chem. Chem. Phys.*, 2024, **26**, 14228

Extension of nature's NIR-I chromophore into the NIR-II region†

Kittipan Siwawannapong,[a] James R. Diers,[b] Nikki Cecil M. Magdaong,[c] Phattananawee Nalaoh,[d] Christine Kirmaier,[c] Jonathan S. Lindsey,*[a] Dewey Holten*[c] and David F. Bocian*[b]

The development of chromophores that absorb in the near-infrared (NIR) region beyond 1000 nm underpins numerous applications in medical and energy sciences, yet also presents substantial challenges to molecular design and chemical synthesis. Here, the core bacteriochlorin chromophore of nature's NIR absorbers, bacteriochlorophylls, has been adapted and tailored by annulation in an effort to achieve absorption in the NIR-II region. The resulting bacteriochlorin, **Phen^{2,1}-BC**, contains two annulated naphthalene groups spanning *meso*,β-positions of the bacteriochlorin and the 1,2-positions of the naphthalene. **Phen^{2,1}-BC** was prepared *via* a new synthetic route. **Phen^{2,1}-BC** is an isomer of previously examined **Phen-BC**, which differs only in attachment *via* the 1,8-positions of the naphthalene. Despite identical π-systems, the two bacteriochlorins have distinct spectroscopic and photophysical features. **Phen-BC** has long-wavelength absorption maximum (912 nm), oscillator strength (1.0), and S_1 excited-state lifetime (150 ps) much different than **Phen^{2,1}-BC** (1292 nm, 0.23, and 0.4 ps, respectively). These two molecules and an analogue with intermediate characteristics bearing annulated phenyl rings have unexpected properties relative to those of non-annulated counterparts. Understanding the distinctions requires extending concepts beyond the four-orbital-model description of tetrapyrrole spectroscopic features. In particular, a reduction in symmetry resulting from annulation results in electronic mixing of *x*- and *y*-polarized transitions/states, as well as vibronic coupling that together reduce oscillator strength of the long-wavelength absorption manifold and shorten the S_1 excited-state lifetime. Collectively, the results suggest a heuristic for the molecular design of tetrapyrrole chromophores for deep penetration into the relatively unutilized NIR-II region.

Received 22nd February 2024,
Accepted 21st April 2024

DOI: 10.1039/d4cp00779d

rsc.li/pccp

Introduction

The near-infrared (NIR) spectral region is of great interest owing to a confluence of research objectives ranging from medical to energy sciences. The NIR is of interest in medicine given the deep penetration of NIR light into soft tissue, which holds potential for imaging and therapeutic applications.[1] Interest in the NIR for energy sciences arises due to the large number of solar photons in this region.[2,3] The NIR is now divided into the NIR-I (700–1000 nm) and the NIR-II (1000–1700 nm) regions.[4] Most work to date has focused on the development of chromophores that absorb in the NIR-I region although the NIR-II region has become a target for active research.[5–9] The recent emphasis on the NIR-II region reflects the longstanding progression of the field of photochemistry – including fundamental studies and chromophore function – across the ultraviolet (UV) and visible (VIS), and into the NIR spectral regions.

Nature's chosen molecules for solar light harvesting are hydroporphyrins, namely chlorophylls and bacteriochlorophylls. The long-wavelength absorption band of chlorophylls lies predominantly in the red region (~640–710 nm), whereas that of bacteriochlorophylls is in the NIR-I region (~750–800 nm).[10] Such values of the long-wavelength band are for the isolated pigments in organic solvents. Longer wavelengths of absorption are obtained in native pigment–protein assemblies.[11–13] The long-wavelength absorption band of the native hydroporphyrins tends to have a large molar absorption coefficient, namely

[a] *Department of Chemistry, North Carolina State University, Raleigh, NC 27695-8204, USA. E-mail: jlindsey@ncsu.edu*
[b] *Department of Chemistry, University of California, Riverside, CA, 92521-0403, USA. E-mail: david.bocian@ucr.edu*
[c] *Department of Chemistry, Washington University, St. Louis, MO, 63130-4889, USA. E-mail: holten@wustl.edu*
[d] *Department of Chemistry, University of Tennessee, Knoxville, TN 37996, USA*

† Electronic supplementary information (ESI) available: Exploratory syntheses; photophysical data for bacteriochlorins; results of TDDFT calculations; ^{1}H and ^{13}C{^{1}H} NMR spectra of new compounds; and single-crystal X-ray data. CCDC 2327783 (**3**), 2327784 (**5**), and 2327785 (**7**). For ESI and crystallographic data in CIF or other electronic format see DOI: https://doi.org/10.1039/d4cp00779d

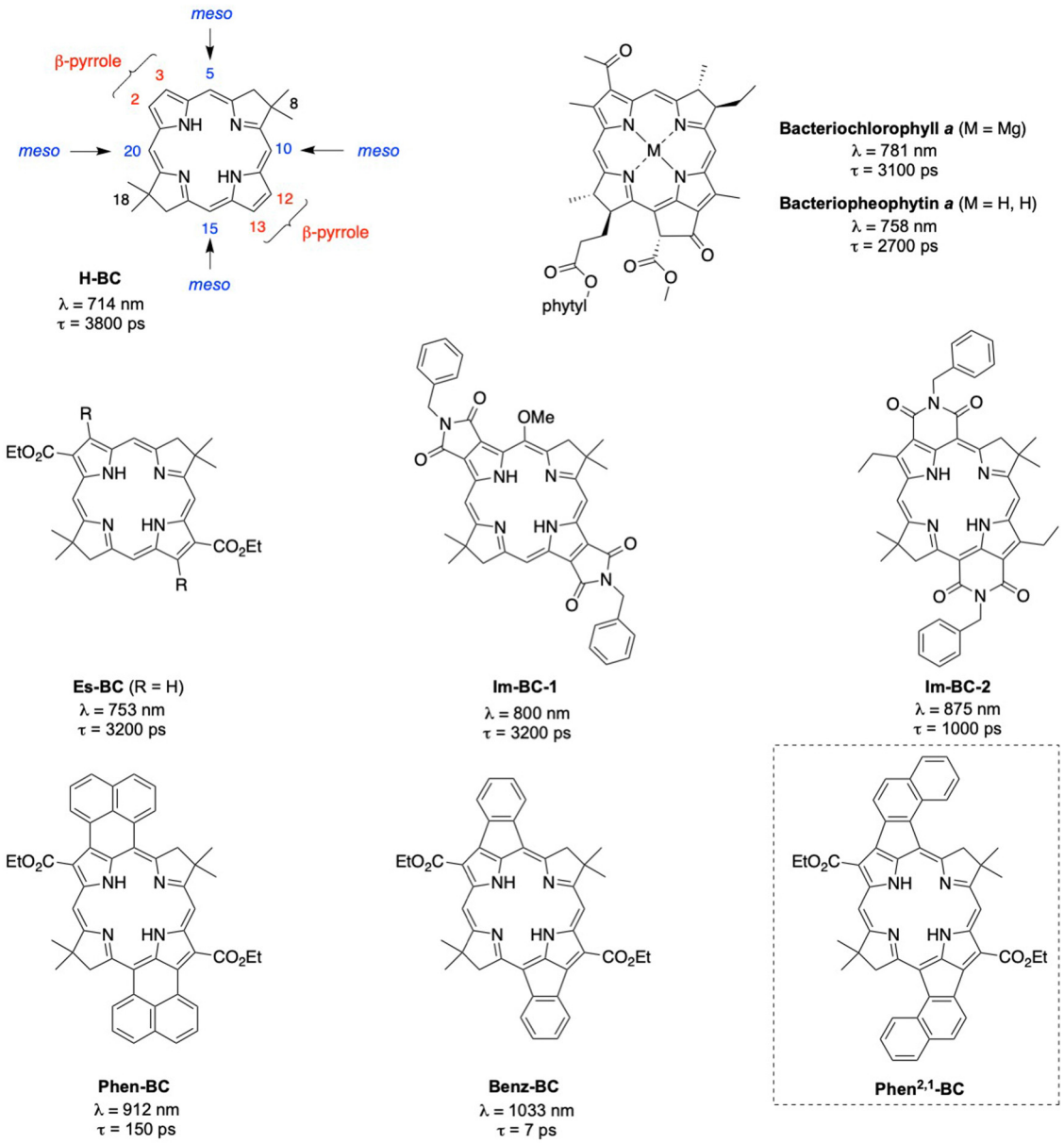

Chart 1 Synthetic and natural bacteriochlorins.

$\sim$100 000 M^{-1} cm^{-1},[10] making them well suited for diverse applications.

Efforts to extend the position of the long-wavelength absorption have been carried out to understand the limits of spectroscopic malleability of the core hydroporphyrin chromophores. A general rule of thumb for the molecular designer is that the more extended the π-system, the longer the wavelength.[14] The notion of extended π-systems dates to fundamental studies of the relationship between color and constitution of synthetic dyes.[15–18] Critical exceptions to this heuristic are known, however, including the effects of macrocycle type (porphyrin *vs.* chlorin *vs.* bacteriochlorin) and specific peripheral-substituent patterns on the spectra of tetrapyrrole chromophores.[14,19]

Over the years, we have been working to understand the effects of conjugated groups on the spectroscopic and photophysical features of synthetic bacteriochlorin analogues of native bacteriochlorophylls.[20] Representative synthetic bacteriochlorins are shown in Chart 1. Each contains a *gem*-dimethyl group (8- and 18-positions) in the reduced ring to secure the chromophore from adventitious dehydrogenation in an aerobic environment. The bacteriochlorin **H-BC** contains no substituents at the β-pyrrole (2,3,12,13) or *meso* (5,10,15,20) positions. Annulation of conjugated groups across adjacent β-pyrrole positions (**Im-BC-1**) or β,*meso*-positions (**Im-BC-2**) with imides[20] causes a significant bathochromic shift of the long-wavelength ($S_0 \rightarrow S_1$) band from that of **H-BC** (714 nm) to 800 or 875 nm, respectively. Even more pronounced spectral shifts are observed upon incorporation of annulated arenes to give **Phen-BC** and **Benz-BC**, which exhibit Q_y maxima at 912 and 1033 nm, respectively.[21] The excited-state lifetimes are also shortened with increasing wavelength along this

series: 3800 ps (**H-BC**), 3200 ps (**Im-BC-1**),[20] 1000 ps (**Im-BC-2**), 150 ps (**Phen-BC**), and 7 ps (**Benz-BC**).[21]

Recently, we performed a series of density functional theory (DFT) calculations that examined nearly 100 designs that might extend the $S_0 \rightarrow S_1$ band deeper into the NIR-II region. One design that appeared synthetically tractable, **Phen^{2,1}-BC** (Chart 1), was calculated to have a Q_y band at 1277 nm. In this paper, the synthesis of **Phen^{2,1}-BC** is described followed by photophysical characterization and theoretical analysis. Compound **Phen^{2,1}-BC** exhibits a $S_0 \rightarrow S_1$ absorption band at 1292 nm but with diminished intensity *versus* expectations. Bacteriochlorins **Phen-BC** and **Phen^{2,1}-BC** are isomers that have an identical number of π-bonds, but differ in the sites of connection to the annulated naphthalene unit. Yet these two isomers exhibit profoundly different absorption spectra and excited-state lifetimes. Efforts to understand the photophysical features of **Phen^{2,1}-BC** have led to new insights concerning both hydroporphyrin spectroscopy and molecular design of annulated hydroporphyrins with potentially deeper NIR absorption.

Results

Synthesis

The prior synthesis of annulated bacteriochlorins **Phen-BC** and **Benz-BC** relied on the approach shown in Scheme 1.[21] A bromo-substituted dihydrodipyrrin (**I**)[21] was converted *via* a Northern–Southern route[22] to the corresponding 2,12-dibromobacteriochlorin (**II**). For annulation, the latter was treated with the arene, which contained one bromine atom and one boronic acid moiety that together define the spacing of adjacent annulation sites. The annulation entailed a two-step process: (1) Suzuki coupling[23] of the 2,12-dibromobacteriochlorin (**II**) with the arene-boronic acid to attach the arene at the bacteriochlorin 2,12-positions, and (2) Heck coupling[24] of the arene-bromide with the bacteriochlorin *meso*-carbons (5,15-positions). Thus, reaction with naphthalene **III** gave **Phen-BC**, whereas benzene **IV** gave **Benz-BC**. Attempts to use naphthalene **V** (prepared herein), however, gave a very poor yield in the Suzuki coupling process. A general challenge was to obtain sufficient 2,12-dibromobacteriochlorin (**II**) for expansive studies of reaction conditions that might ameliorate the coupling with **V**. An alternative route to 2,12-dibromobacteriochlorin (**II**) was explored beginning with pyrrole **VI** and synthon **VII** to obtain a bromo-substituted dihydrodipyrrin (**VIII**) for use *via* an Eastern–Western route,[22] but this approach was not fruitful. The synthetic approaches *via* **II** to obtain annulated bacteriochlorins were discontinued (see ESI,† Section S1).

A new route was developed to gain access to the target bacteriochlorin **Phen^{2,1}-BC** (Scheme 2). The route entails incorporation of a bromonaphthyl group at the beginning of the synthesis, and relies on the Eastern–Western approach to construct the bacteriochlorin macrocycle. After exploratory studies of a four-component approach to the requisite bromoarene-pyrrole,[25] a two-component approach[26] was pursued. Thus, reaction of 1-bromo-2-(2-nitrovinyl)naphthalene (**1**)[27] and β-enamino ester **2** was carried out to afford pyrrole **3**. Study of reaction conditions identified use of overnight reflux in toluene[25] (containing 20 mol% $FeCl_3$ relative to **1**), which afforded **3** in 47% yield (see the ESI,† Section S1 for reaction surveys[28]). The structure of **3** was confirmed by X-ray crystallography (Fig. 1(A)).

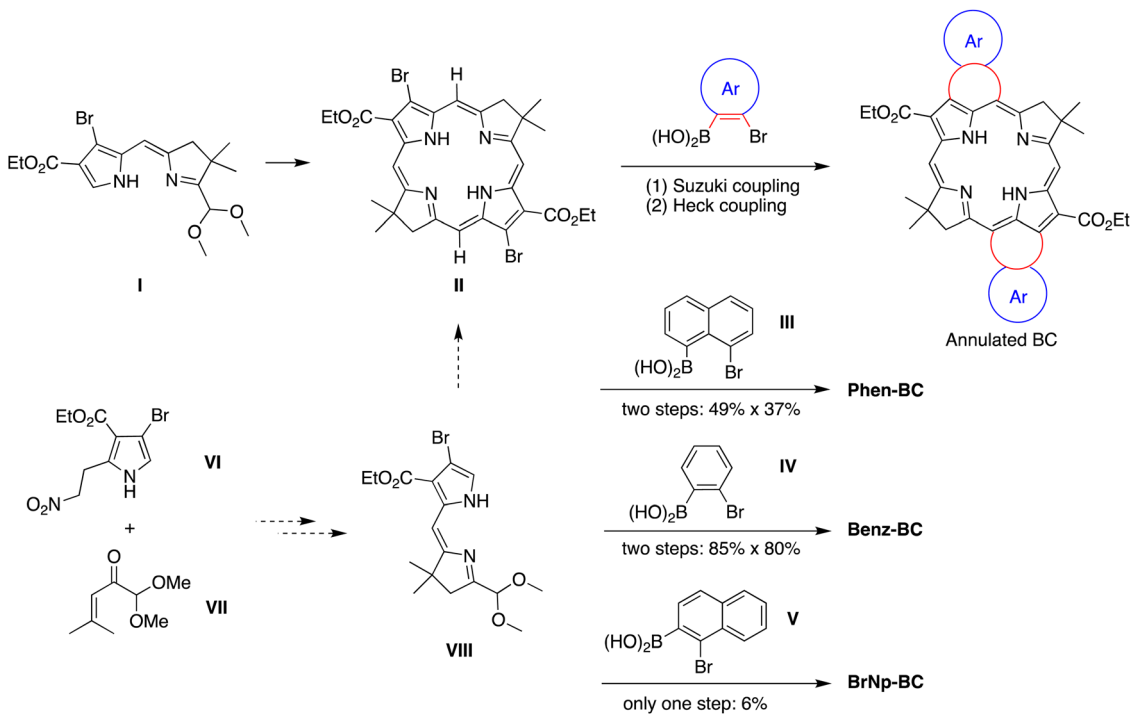

Scheme 1 Synthesis routes to annulated bacteriochlorins.

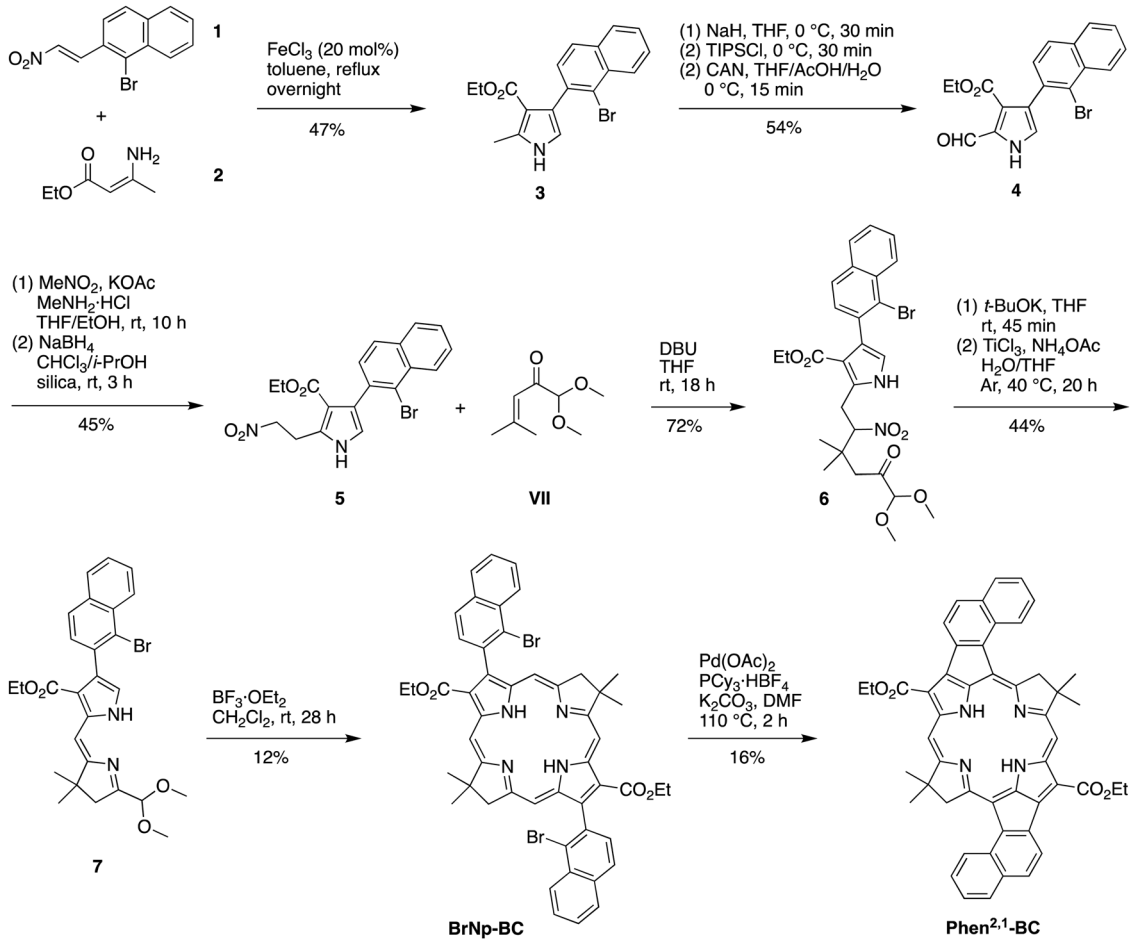

Scheme 2 Synthesis of annulated bacteriochlorin **Phen^{2,1}-BC**.

The subsequent transformations to form the corresponding dihydrodipyrrin follow those for the Eastern–Western route. Thus, pyrrole **3** was converted[29] to the *N*-TIPS derivative followed by oxidation of the 2-methyl group using ceric ammonium nitrate (CAN)[30] to give the 2-carboxaldehyde **4** in 54% yield. Henry reaction[31] with nitromethane and subsequent reduction[29] with $NaBH_4$ gave the 2-(2-nitroethyl)pyrrole **5** in 45% yield. The structure of **5** was confirmed by X-ray crystallography (Fig. 1(B)). Michael addition[32] of **5** and α,β-unsaturated ketone **VII**[33] under known conditions[29,34] gave the nitrohexanone **6** in 72% yield. Cyclization[29,34] of **6** using potassium *tert*-butoxide followed by addition of $TiCl_3$ in the presence of ammonium acetate (McMurry–Melton reaction)[35,36] gave dihydrodipyrrin **7** in 44% yield. The structure of **7** was confirmed by X-ray crystallography (Fig. 1(C)). Self-condensation[29] of **7** was carried out with catalysis by $BF_3{\cdot}OEt_2$ at room temperature, which gave (as expected)[22] bacteriochlorin **BrNp-BC** as a single band (for evidence of atropisomers, see the Experimental section) in 12% yield.

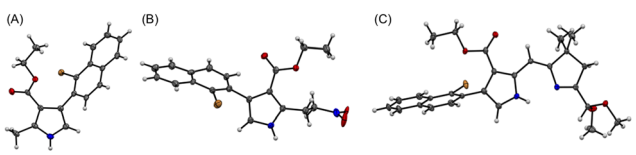

Fig. 1 ORTEP drawing of the single crystal X-ray structures of (A) bromonaphthyl-bearing pyrrole **3**, (B) the intermediate **5**, and (C) dihydrodipyrrin **7**. All ellipsoids are contoured at the 50% level. Disordered units are omitted for clarity (Label: C = grey, N = blue, O = red, Br = orange, H = white).

The Heck reaction[24] of **BrNp-BC** was carried out using $Pd(OAc)_2$ and the ligand tricyclohexylphosphonium (PCy_3) tetrafluoroborate in *N*,*N*-dimethylformamide (DMF) at 110 °C, the same conditions used previously[21] for formation of **Phen-BC** and **Benz-BC**. The desired doubly annulated bacteriochlorin **Phen^{2,1}-BC** was obtained in 16% yield. The composition of **Phen^{2,1}-BC** was confirmed by accurate mass analysis, and the structure was analyzed by a battery of 2D NMR methods (ESI,† Section S11). Analysis by 1D ^{1}H NMR spectroscopy (in $CDCl_3$) showed a singlet at 3.21 ppm, attributed to the resonance of the N–H protons, which can be compared with those for annulated bacteriochlorins **Phen-BC** (1.97 ppm) and **Benz-BC** (2.89 ppm).[21] In perspective, the resonance of the N–H protons in the ~2–3 ppm region is unusual, given that most tetrapyrrole macrocycles (and bacteriochlorins) lacking annulation tend to resonate in the far upfield region (–1 to –3 ppm). Comparison of the ^{1}H NMR chemical shifts of the three annulated bacteriochlorins with two benchmark bacteriochlorins is provided in Table 1. The change in chemical shifts suggests progressively weaker ring currents

Table 1 ^{1}H NMR Chemical shifts of bacteriochlorins

	Chemical shifts (ppm)				
Hydrogens	**H-BC**[37]	**EtEs-BC**[a 38]	**Benz-BC**[21]	**Phen-BC**[21]	**Phen^{2,1}-BC**
meso-H	8.73 8.83	8.64 9.66	8.71	8.35	7.77
gem-Dimethyl	1.97	1.94	1.78	1.57	1.20
N–H	−2.38	−1.43	2.89	1.97	3.21
pyrroline CH_2	4.47	4.78	4.00	4.31	3.49

[a] 2,12-Bis(carboethoxy)-3,13-diethyl-8,8,18,18-tetramethylbacteriochlorin (R = Et in Chart 1).

among the annulated bacteriochlorins in the series **Phen-BC** > **Benz-BC** > **Phen^{2,1}-BC**.

In summary, the synthesis of **Phen^{2,1}-BC** described herein entailed development of a new route (Scheme 2) with the following advantages *versus* the prior route (Scheme 1): (1) use of one Pd-coupling reaction (Heck) rather than a sequence of two Pd coupling reactions (Suzuki and Heck), which required a large excess of the bromo-arene-boronic acid to avoid competitive coupling processes; (2) no requirement to synthesize a bromo-arene-boronic acid (which is facile for **III** and **IV**, but not for **V** or perhaps other annulation partners); and (3) avoidance of bromination of the pyrrole moiety leading to the dihydrodipyrrin. On the other hand, one disadvantage is the requirement to install the annulation motif (*i.e.*, the bromonaphthalene unit) at the first step of the synthesis.

Absorption spectra

Fig. 2(A) shows electronic absorption spectra of six bacteriochlorins (Chart 1 and Scheme 2) in toluene at room temperature. The $S_0 \rightarrow S_1$ vibronic manifold for each molecule is shaded. The spectra are labeled with the $S_0 \rightarrow S_1$ oscillator strengths obtained from time-dependent DFT (TDDFT) calculations (*vide infra*).[39] This method affords a $S_1(0,0)$ peak intensity ratio of 22 for **BrNp-BC** *vs.* **Phen^{2,1}-BC**, in good agreement with the ratio of 21 for the measured molar absorption coefficients (see Experimental section). The $S_0 \rightarrow S_1$ manifolds are normalized to the peak intensity in Fig. 2(B) (solid). The wavelengths and energy spacing of the spectral features are summarized in Table 2. The $S_1(0,0)$ band of non-annulated bacteriochlorins **H-BC** (714 nm), **Es-BC** (753 nm), and **BrNp-BC** (771 nm) is characteristically sharp and intensifies and shifts bathochromically along this series. At progressively higher energy are the weak $S_2(0,0)$ band (490–530 nm) and strong $S_3(0,0)$ (365–380 nm) and $S_4(0,0)$ (340–360 nm) bands. The characteristics of these features can be understood within Gouterman's four-orbital model (*vide infra*).[19,40,41] The standard assignments for the non-annulated bacteriochlorins are $S_0 \rightarrow S_1$ (Q_y), $S_0 \rightarrow S_2$ (Q_x), $S_0 \rightarrow S_3$ (B_x), and $S_0 \rightarrow S_4$ (B_y).

In contrast, TDDFT calculations show that the four-orbital model is not applicable for the annulated bacteriochlorins such as **Benz-BC** and **Phen^{2,1}-BC** because the $S_0 \rightarrow S_1$ and $S_0 \rightarrow S_2$

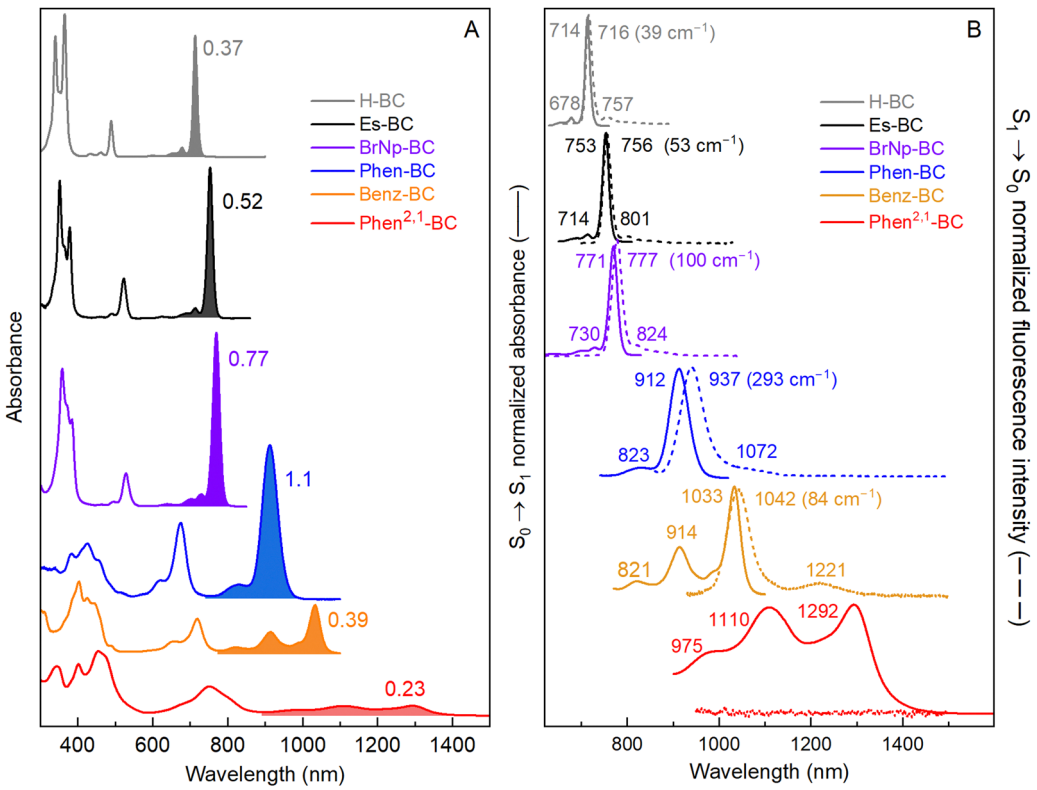

Fig. 2 (A) Absorption spectra of **H-BC** (grey), **Es-BC** (black), **BrNp-BC** (violet), **Phen-BC** (blue), **Benz-BC** (gold), and **Phen^{2,1}-BC** (red). The $S_0 \rightarrow S_1$ vibronic manifold is shaded. The oscillator strength of the $S_0 \rightarrow S_1$ manifold obtained from TDDFT calculations is given. (B) Absorption spectra (solid) and fluorescence spectra (dashed) of the bacteriochlorins normalized at the largest peak. The value in parenthesis is the absorption–fluorescence (Stokes) shift.

Table 2 Photophysical and electronic properties of the bacteriochlorins[a]

Property	Units	H-BC	Es-BC	BrNp-BC	Phen-BC	Benz-BC	Phen^{2,1}-BC
S_1 absorption							
$S_1(0,0)$	nm	714	753	771	912	1033	1292
$S_1(1,0)$	nm	678	714	730	823	914	1110
$S_1(2,0)$	nm	649	678	695		818	975
$S_1(1,0)$–$S_1(0,0)$	cm^{-1}	744	725	728	1142	1260	1269
$S_1(2,0)$–$S_1(1,0)$	cm^{-1}	659	744	690		1239	1247
S_2 absorption							
$S_2(0,0)$	nm	489	523	529	675	718	812
$S_2(1,0)$	nm	462	490	496	619	654	750
$S_2(2,0)$	nm	433	460	463	571	600	678
$S_2(1,0)$–$S_2(0,0)$	cm^{-1}	1195	1288	1258	1340	1363	1018
$S_2(2,0)$–$S_2(1,0)$	cm^{-1}	1450	1331	1437	1358	1376	1223
S_1 emission							
$S_1(0,0)$	nm	716	756	777	937	1042	[b]
$S_1(0,1)$	nm	757	801	824	1072	1221	[b]
$S_1(1,0)$–$S_1(0,0)$	cm^{-1}	756	743	734	1344	1407	[b]
Differences							
$S_1(0,0)$ Ab-Em	cm^{-1}	39	53	100	293	84	[b]
$S_2(0,0)$–S_1 (0,0) Ab	cm^{-1}	6444	5840	5933	3850	4247	4575
Excited state[c]							
Φ_f		0.14	0.19	0.029	0.004	2.3×10^{-4}	$<3 \times 10^{-5}$
τ_S	ps	3800	3200	500	150	7	0.4
k_{IC}	ps^{-1}	17 000	11 000	4200	152	7	0.4
Electronic structure[d]							
S_1–S_2 TDM θ_{12}	degrees	90	73	89	55	46	39
f_1		0.37	0.52	0.75	1.0	0.39	0.23
f_2		0.11	0.19	0.18	0.31	0.41	0.53
f_1/f_2		3.4	2.7	4.2	3.2	0.95	0.43

[a] See Chart 1 and Scheme 2 for chemical structures. All measurements were made in toluene at room temperature. [b] No emission observed. [c] Excited-state properties are from the literature for **Phen-BC**,[21] **Es-BC**,[42] and **H-BC**.[43] [d] From TDDFT calculations. The $S_0 \rightarrow S_1$ and $S_0 \rightarrow S_2$ oscillator strengths are f_1 and f_2, respectively.

transitions have mixed *x*–*y* polarization (*vide infra*). One indicator that the four-orbital model is not operative is the dramatically diminished intensity of the $S_0 \rightarrow S_1$ manifold along the series **Phen-BC** > **Benz-BC** > **Phen^{2,1}-BC** as the features move to longer wavelengths (Fig. 2 and Table 2). Moreover, the $S_1(1,0)$ band (1110 nm) and $S_2(1,0)$ band (750 nm) of **Phen^{2,1}-BC** and the $S_1(1,0)$ band (914 nm) of **Benz-BC** are more intense than expected for a Franck–Condon progression. These observations indicate vibronic coupling significantly impacts the $S_0 \rightarrow S_1$ and $S_0 \rightarrow S_2$ manifolds of **Phen^{2,1}-BC** and **Benz-BC**. The nature of the vibronic progressions are also altered by annulation. A $\sim$1300 cm^{-1} vibronic spacing (stretching vibrations[19]) dominates the $S_0 \rightarrow S_1$ manifolds of **Phen-BC**, **Benz-BC**, **Phen^{2,1}-BC** compared to the dominant spacing of $\sim$730 cm^{-1} (an accordion-like mode[44]) in the $S_0 \rightarrow S_1$ manifold of **H-BC**, **Es-BC**, and **BrNp-BC** (Table 2). Spectra of **Benz-BC** and **Phen^{2,1}-BC** at 77 K show, in addition to the primary $\sim$1300 cm^{-1} spacing, a weaker progression built on an $\sim$500 cm^{-1} mode (ESI,† Fig. S2 and Table S6). The latter could be an accordion-like mode down-shifted in energy due to the added mass of the annulated rings.

Fluorescence spectra and quantum yields

Fig. 2(B) zooms in on the $S_0 \rightarrow S_1$ absorption manifolds (solid) of the six bacteriochlorins and shows the corresponding $S_1 \rightarrow S_0$ fluorescence manifolds (dashed). Peak positions and energy spacings are summarized in Table 2. The typical small Stokes shifts between the $S_1(0,0)$ absorption and fluorescence maxima are found for **H-BC** (39 cm^{-1}), **Es-BC** (53 cm^{-1}), and **BrNp-BC** (100 cm^{-1}). In each case, the fluorescence spectrum is mirror image to the absorption spectrum in terms of both relative intensities and dominant spacing ($\sim$730 cm^{-1}) of the vibronic bands.

Annulated **Phen-BC** shows a moderate (293 cm^{-1}) Stokes shift with mirror symmetry of the fluorescence and absorption manifolds. On the other hand, the intensity profile in the fluorescence manifold of **Benz-BC** is not mirror symmetric to that in the absorption manifold (Fig. 2(B), gold). This reinforces the view that the (1,0) band in the $S_0 \rightarrow S_1$ absorption manifold of **Benz-BC** gains considerable strength *via* vibronic coupling. Turning to **Phen^{2,1}-BC**, it is apparent from Fig. 2(B), and measurements extending to 1700 nm presented in ESI,† Section S4, that fluorescence from the new annulated bacteriochlorin is too weak to be observed. Thus, the fluorescence quantum yield (Φ_f) of **Phen^{2,1}-BC** is $<3 \times 10^{-5}$, using *meso*-tetraphenylporphyrin in non-degassed toluene (Φ_f = 0.070)[45] or **Phen-BC** in Ar-purged toluene (Φ_f = 0.004)[21] as standards. Here, $\Phi_f = 2.3 \times 10^{-4}$ for **Benz-BC** was determined, updating a value found previously where emission was barely observed and the vibronic manifold not resolved.[21] The Φ_f values of two other bacteriochlorins determined previously are 0.14 for **H-BC**,[43] and 0.13 for **Es-BC**.[42] The low Φ_f value found here of 0.029 for **BrNp-BC** is attributed to a heavy atom effect of the bromines (Scheme 2) on $S_1 \rightarrow T_1$ intersystem crossing, consistent with transient absorption studies (ESI,† Section S6).

Excited-state decay properties

Transient-absorption difference spectra and kinetics for Phen^{2,1}-BC. Fig. 3(A) shows transient absorption (TA) difference

spectra for **Phen^{2,1}-BC** in toluene at several times after excitation. The dashed vertical line indicates that the data acquired in the nominal "visible" region (~400–815 nm) and the NIR region (~815–1450 nm) were joined. Fig. 3(B) gives the ground-state absorption spectrum as a reference and a representative kinetic profile and fit (inset). The TA difference spectrum for **Phen^{2,1}-BC** at 0.3 ps (Fig. 3(A), blue trace) shows bleaching of the ground-state absorption at 450, 750, 1110, and 1295 nm, as well as excited-state absorption bands at 530 and 875 nm. Excited-state stimulated emission may contribute to the negative-going feature at 1295 nm. By 10 ps (red trace), the ground-state bleaching features at 1110 and 1295 nm have decayed to ~25% of the initial amplitude and the excited-state absorption bands at 530 and 875 nm have decayed to 10%. The spectra have reached the $\Delta A = 0$ line by 50 ps (gold trace). The inset to Fig. 3(B) and Fig. S9 (ESI†) give kinetic traces with average fit time constants of ~0.4 ps and ~12 ps.

The TA data sets were subjected to global analysis presented in ESI,† Section S5 in which several kinetic models were tested. The analysis is most consistent with Model D (Fig. S7, ESI†), in which the lowest excited singlet state (S_1) of **Phen^{2,1}-BC** decays by internal conversion to S_0 with a time constant of ~0.4 ps. This rapid downhill (~1 eV) decay produces a vibrationally "hot" S_0 that "cools" with τ ~12 ps by flow of the excess energy into the solvent. A time scale of ~10 ps or longer has been found for vibrational cooling of large aromatic systems[46–53] including tetrapyrroles.[54,55] Also, the S_1 excited state itself likely has not vibrationally relaxed prior to internal conversion because internal vibrational redistribution of such systems often takes >1 ps.[46,47,50–52] The results for **Phen^{2,1}-BC** can be compared with those for **H-BC**,[43] **Es-BC**,[42] **BrNp-BC** (ESI,† Section S6), and **Phen-BC**.[21] The S_1 excited-state lifetimes are 3.8 ns, 3.3 ns, 500 ps and 150 ps, and the rate constants for $S_1 \rightarrow S_0$ internal conversion are $(17\ ns)^{-1}$, $(11\ ns)^{-1}$, $(4.2\ ns)^{-1}$ and $(152\ ps)^{-1}$, respectively (Table 2).

Energy-gap law for internal conversion. The ~0.4 ps $S_1 \rightarrow S_0$ internal conversion for **Phen^{2,1}-BC** gives the closed blue diamond (point 16D) in Fig. 4. This value is longer than the ~50-fs extrapolated (blue line) from results for other bacteriochlorins including **Benz-BC** and **Phen-BC** in which the annulation spans the *meso*,β-positions (Chart 1).[21] The measured ~0.4 ps is longer than the extrapolated ~50 fs because internal vibrational relaxation within S_1 is likely convolved with internal conversion to S_0. The structures of all compounds cited in Fig. 4 are displayed in Chart S1 (ESI,† Section S5).

In ESI,† Section S5, a less-favored interpretation of the TA data for **Phen^{2,1}-BC** is considered in which the $S_1 \rightarrow S_0$ internal conversion time is ~12 ps (and prior relaxation within S_1 taking ~0.4 ps). This Model C gives the blue open diamond (denoted 16C) in Fig. 4. This time is shorter than the 70 ps extrapolated (red line) for "normal" bacteriochlorins. Similarly, the measured 7 ps for **Benz-BC** (point 15)[21] is shorter than the extrapolated 400 ps. A smaller difference exists for **Phen-BC** (point 14). Collectively, the results obtained herein for **Phen^{2,1}-BC** along with those for **Phen-BC** and **Benz-BC** show that β-*meso* annulation results in $S_1 \rightarrow S_0$ internal conversion rates enhanced from those expected on the basis of energy-gap-law considerations for most bacteriochlorins.

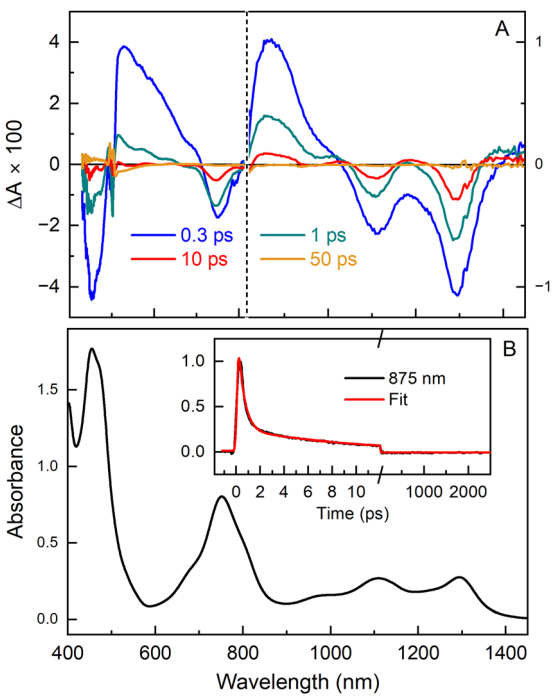

Fig. 3 (A) Representative TA spectra for **Phen^{2,1}-BC** at select delay times after excitation at 500 nm; (B) ground-state absorption spectrum and kinetic profile and dual-exponential fit at 875 nm. The vertical dashed lines in panel A mark the cutoff between the visible and NIR data, the latter using a 4× smaller ΔA scale (see left and right vertical axes).

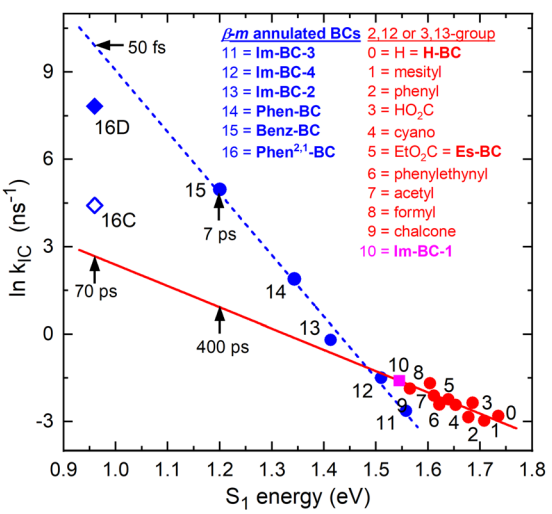

Fig. 4 Energy-gap law plot showing the natural logarithm of the rate constant for $S_1 \rightarrow S_0$ internal conversion *versus* the S_1 energy for various bacteriochlorins. The blue line is a fit for bacteriochlorins bearing one or two imide moieties or annulated rings spanning adjacent *meso* and β-pyrrole positions, including **Phen-BC** and **Benz-BC** (Chart 1). The blue line projects a time constant of ~50 fs for **Phen^{2,1}-BC**. The red line is a fit for ten benchmark bacteriochlorins (ESI,† Chart S1) and one β,β-annulated imide-bacteriochlorin (point 10).

Electronic-structure calculations

Molecular orbital characteristics from DFT. The energies and electron densities of the frontier MOs of the six bacteriochlorins (Chart 1 and Scheme 2) are shown in Fig. 5. Additional MOs for each molecule are given in ESI,† Section S7. The two highest occupied orbitals (HOMO and HOMO−1) and the two lowest unoccupied orbitals (LUMO and LUMO+1) for **H-BC** (Fig. 5(A)), **Es-BC** (Fig. 5(B)), and **BrNp-BC** (Fig. 5(C)) are the MOs of Gouterman's four-orbital model (*vide infra*).[19,40,41] The MOs of **Phen-BC**, **Benz-BC**, and **Phen^{2,1}-BC** have electron density distributions at the macrocycle positions that are generally similar (but not identical) to those for the non-annulated benchmarks, in addition to density delocalized onto the annulated rings.

Excited-state properties calculated by TDDFT. Fig. 6 compares the measured $S_0 \rightarrow S_1$ and $S_0 \rightarrow S_2$ absorption manifolds (brown) with the spectrum calculated by TDDFT (sticks and dashed blue line) for each bacteriochlorin. Comparisons extending to higher transitions ($S_0 \rightarrow S_8$) into the near-UV region are given in ESI,† Section S8.

The TDDFT calculations reproduce well the measured spectra, with the caveat that these calculations do not account for vibronic satellite bands. In particular, the calculations capture the bathochromic shift of the $S_0 \rightarrow S_1$ manifold along the series **H-BC** < **Es-BC** < **BrNp-BC** < **Phen-BC** < **Benz-BC** < **Phen^{2,1}-BC**. The calculations also reproduce the increase in S_1/S_2 intensity ratio along the first three members and the reverse for the last three members: **H-BC** < **Es-BC** < **BrNp-BC** > **Phen-BC** > **Benz-BC** > **Phen^{2,1}-BC** (Fig. 6 and last row of Table 2).

Fig. 6 also gives the natural transition orbitals (NTOs) for the $S_0 \rightarrow S_1$ and $S_0 \rightarrow S_2$ transitions. ESI,† Section S8 gives the NTOs for higher energy transitions. A pair of occupied and virtual (unoccupied) NTOs reveals the change in electron density involved in a transition.[56] All six bacteriochlorins require two NTO pairs (contribution of two electron promotions), for which the relative weights are given next to the arrows in Fig. 6. The occupied NTOs for the $S_0 \rightarrow S_1$ and $S_0 \rightarrow S_2$ transitions of **H-BC** (Fig. 6(A)) are the same as the filled frontier MOs (HOMO and HOMO−1) (Fig. 5(A)). The same is

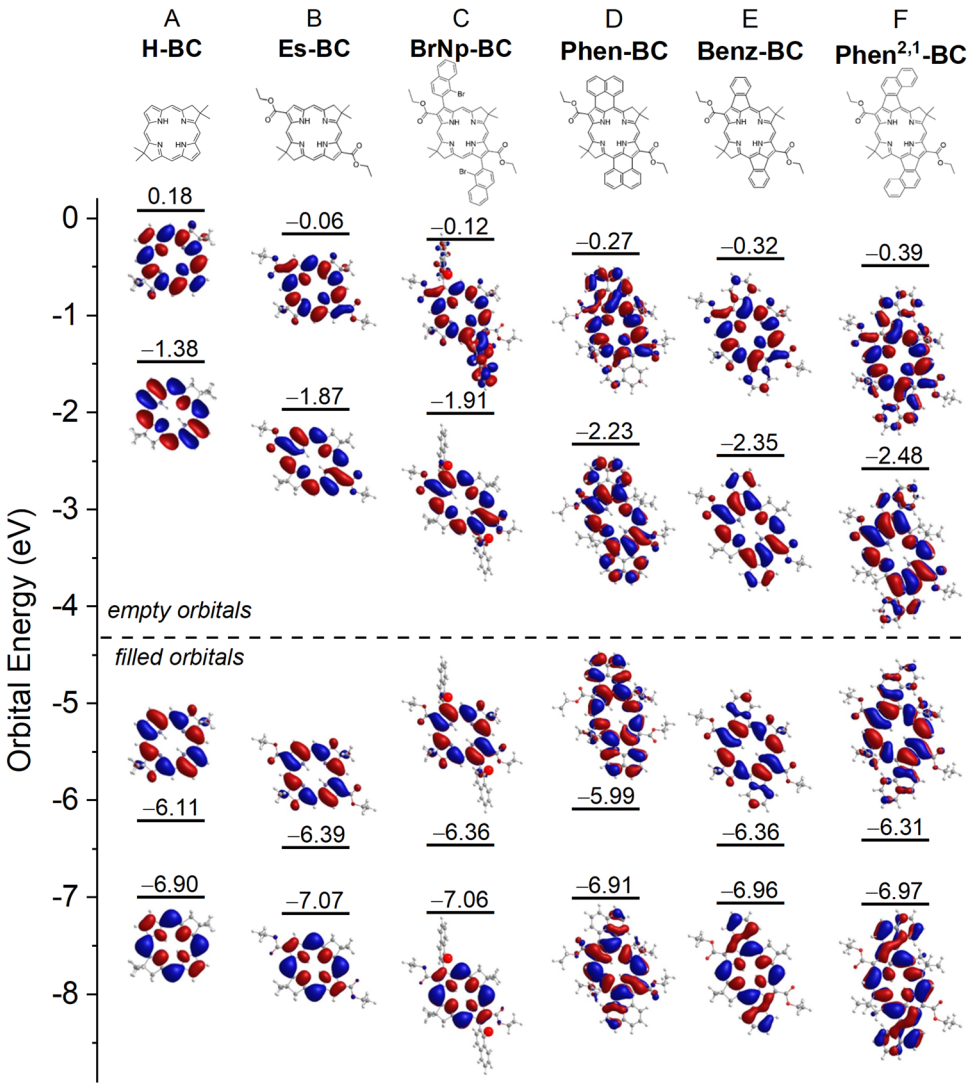

Fig. 5 Frontier MO correlation diagram for six bacteriochlorins.

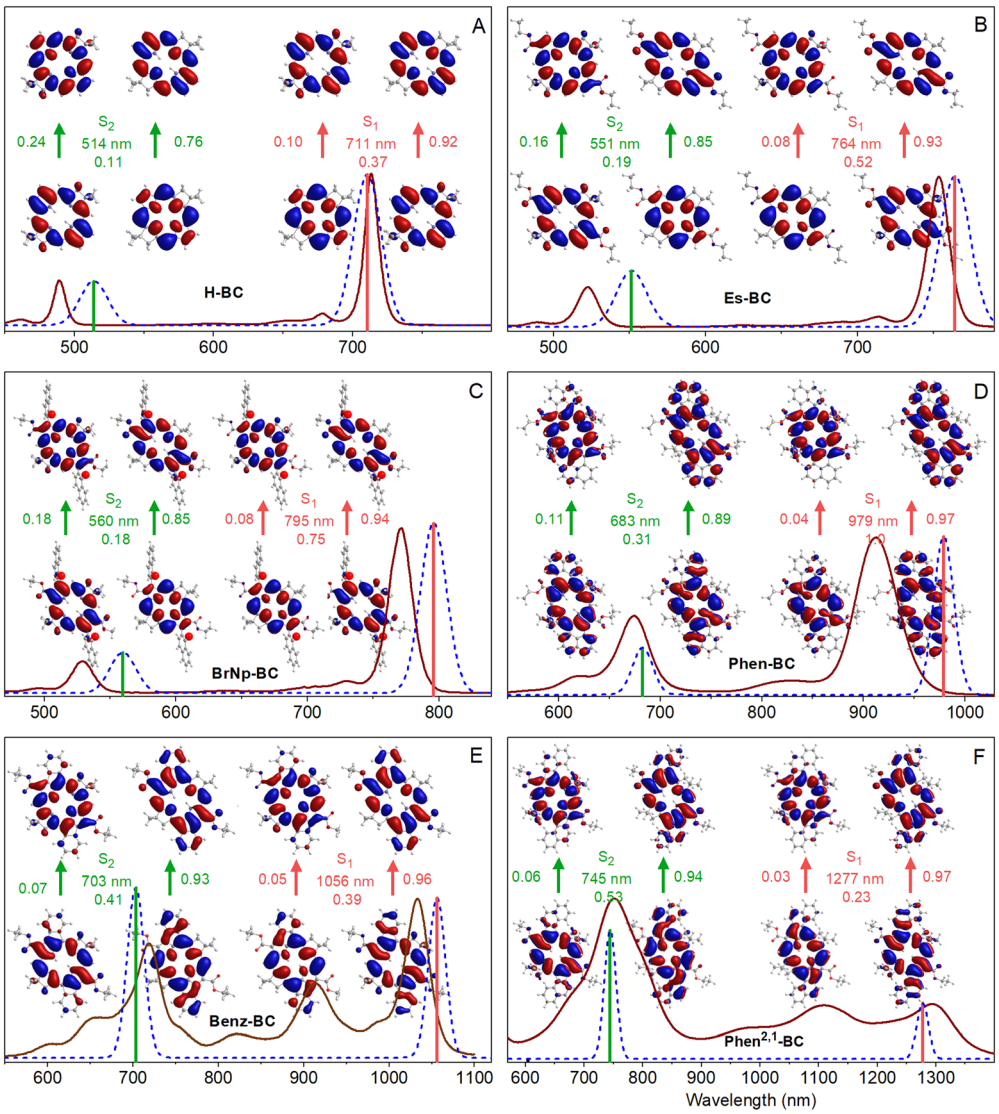

Fig. 6 Comparison for (A) **H-BC**, (B) **Es-BC**, (C) **BrNp-BC**, (D) **Phen-BC**, (E) **Benz-BC**, and (F) **Phen^{2,1}-BC** of the absorption spectra in toluene that are measured (brown line) or calculated *via* TDDFT (dashed blue lines and colored sticks) normalized at the $S_0 \rightarrow S_1(0,0)$ peak. Calculated spectral features were given 10-nm Gaussian skirts. Shown for the $S_0 \rightarrow S_1$ and $S_0 \rightarrow S_2$ transitions are the natural transition occupied and virtual orbitals along with the wavelength and oscillator strength of the transition obtained from TDDFT. Two NTO promotions contribute to each transition, with weights indicated by the values that flank the arrows.

true of the virtual NTOs compared to the empty MOs (LUMO and LUMO+1). This close matching of NTOs and MOs also holds for **Es-BC** (Fig. 6(B) *vs.* Fig. 5(B)) and **BrNp-BC** (Fig. 6(C) *vs.* Fig. 5(C)). This reflects the fact that for a given transition there is no common orbital involved in multiple electron promotions.

Setting aside electron delocalization onto the fused ring systems, the electron densities at the macrocycle positions in the MOs (Fig. 5) and NTOs (Fig. 6) for **Phen-BC**, **Benz-BC**, and **Phen^{2,1}-BC** (panels D–F) are generally similar (but not identical) to those for the non-annulated analogues (panels A–C). This seems surprising given (1) the variation in S_1/S_2 intensity ratio described above (Fig. 6) and (2) substantial changes in the transition dipole moment (TDM) directions (Fig. 7). For **H-BC**, the $S_0 \rightarrow S_1$ (Q_y) transition lies along the NH–HN axis, which is the traditional *y*-axis for tetrapyrroles, and the $S_0 \rightarrow S_2$ (Q_x) transition is perpendicular to that ($\theta_{12} = 90^\circ$ in Fig. 7(A)).[19,57] For **Es-BC**, the $S_0 \rightarrow S_2$ transition is rotated somewhat off perpendicular ($\theta_{12} = 73^\circ$) due to the 2,12-ester groups. The flanking 3,13-bis(bromonaphthalene) groups of **BrNp-BC** reintroduce near orthogonality ($\theta_{12} = 89^\circ$). The S_1–S_2 angle difference (θ_{12}) decreases dramatically among the annulated bacteriochlorins: **Phen-BC** (55°) > **Benz-BC** (46°) > **Phen^{2,1}-BC** (39°). The shift of S_1 and S_2 TDM directions from perpendicularity (and off the traditional *x*- and *y*-axes) reflects mixed *x*–*y* compositions of the $S_0 \rightarrow S_1$ and $S_0 \rightarrow S_2$ transitions (*vide infra*).

In spite of the mixed *x*–*y* character implied by the TDM directions, the macrocycle electron distributions of the MOs and NTOs involved in the $S_0 \rightarrow S_1$ transition for the three annulated bacteriochlorins (Fig. 5(D)–(F) and 6(D)–(F))

primarily have the characteristics of those for the non-annulated analogues (Fig. 5(A)–(C) and 6(A)–(C)), which are *y*-polarized (hence the traditional Q_y designation for the non-annulated bacteriochlorins). Similarly, the MOs and NTOs involved in $S_0 \rightarrow S_2$ for the three annulated bacteriochlorins are similar to those for the non-annulated analogs, which are *x*-polarized (normally designated Q_x). Such findings are outside expectations and require in-depth analysis described in the following discussion.

Discussion

The creation of new NIR-II absorbers presents a host of challenges encompassing molecular design, synthesis, photophysics, and theory. The design of **Phen^{2,1}-BC** emerged from prior knowledge of the properties of the annulated bacteriochlorins **Phen-BC** and **Benz-BC** along with subsequent extensive calculations aimed at attaining longer Q_y maxima. Bacteriochlorins **Phen-BC** and **Phen^{2,1}-BC** have identical numbers of π-bonds but are isomeric due to the different sites of connection on the annulated naphthalene rings. It warrants emphasis that the term annulation here refers to an appended group that is conjugated with the macrocycle at two points of attachment. Isomers **Phen-BC** and **Phen^{2,1}-BC** have quite distinct photophysical features (Fig. 2 and Table 2) despite generally similar electron distributions in their frontier orbitals (Fig. 5 and 6). The electron-density distributions in the annulated bacteriochlorins are also generally similar to those of the non-annulated benchmarks. These observations prompt several fundamental questions: (1) how can one explain these seemingly incongruous findings (Fig. 2, 5 and 6)? (2) Is there a connection to the rapid internal conversion rates, and thus short S_1 lifetimes, for the annulated bacteriochlorins (Fig. 4)? The resolution of these issues requires a reexamination of the applicability of the four-orbital model[19,40,41] to tetrapyrrole architectures that include annulations. Accordingly, the subsequent sections are organized as follows: first, the four-orbital model applied to bacteriochlorins is presented; second, the electronic and spectral effects of *x*–*y* mixing are described; and third, the effects of vibronic coupling are considered. Taken together, the results provide new insights concerning hydroporphyrin designs that can afford (strong) absorption in the NIR-II region.

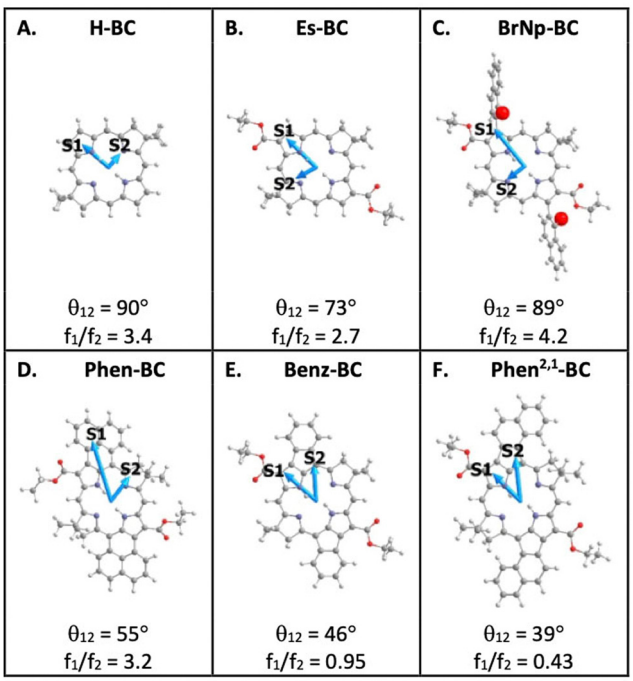

Fig. 7 Calculated TDM directions for the $S_0 \rightarrow S_1$ and $S_0 \rightarrow S_2$ transitions, the angle between them (θ_{12}), and the ratio of oscillator strengths (f_1/f_2) for (A) **H-BC**, (B) **Es-BC**, (C) **BrNp-BC**, (D) **Phen-BC**, (E) **Benz-BC**, and (F) **Phen^{2,1}-BC**. See Chart 1. The calculated ratio of oscillator strengths (f_1/f_2) for the two transitions is also given.

The four-orbital model applied to bacteriochlorins

In Gouterman's four-orbital model,[19,40,41] the $S_0 \rightarrow S_1$ (Q_y) transition derives from the asymmetric linear combination of the HOMO → LUMO and HOMO−1 → LUMO+1 excited-state configurations, both being *y*-polarized. Similarly, the $S_0 \rightarrow S_2$ (Q_x) transition reflects the asymmetric combination of HOMO−1 → LUMO and HOMO → LUMO+1, both being *x*-polarized. The configurational mixing decreases as the energy difference (ΔE) between excited-state configurations increases. For bacteriochlorins such as **H-BC**, ΔE is large, the mixing is small, and $S_0 \rightarrow S_1$ transition has 92% HOMO → LUMO character (Table S7, ESI†). In progressing from **H-BC** to **Es-BC** and **BrNp-BC** (Chart 1), the substituents cause the HOMO → LUMO energy to drop (Fig. 5). The changes in spectral properties along this trio of compounds (Fig. 2) are consistent with the four-orbital-model (ESI,† Section S10). However, the model cannot explain the dramatic decrease in $S_0 \rightarrow S_1$ intensity along the series **Phen-BC** > **Benz-BC** > **Phen^{2,1}-BC** (Fig. 2 and Table 2).

Electronic and spectral effects of *X*–*Y* mixing

The fundamental underpinning of Gouterman's four-orbital model[19,40,41] is that the tetrapyrroles have electron promotions, optical transitions, and excited states that are classified by one of two distinct irreducible representations in the appropriate symmetry group: metalloporphyrins (D_{4h}); free base porphyrins, free base bacteriochlorins and metallobacteriochlorins (D_{2h}); and free base chlorins and metallochlorins (C_{2v}). For all these cases, the promotions, transitions, and excited states relevant to the UV-Vis-NIR spectral properties have one of two symmetry designations, which transform as either *x* or *y* but not a mixture thereof.

The actual symmetry (considering macrocycle and peripheral substituents) of the MOs (and NTOs) for **H-BC**, **Es-BC**, **BrNp-BC**, **Phen-BC**, **Benz-BC**, and **Phen^{2,1}-BC** is not D_{4h}, D_{2h}, or C_{2v}, but rather is C_{2h}. The filled orbitals transform as a_u and the empty orbitals as b_g. The promotions have b_u symmetry and thus could lie anywhere in the *x*–*y* plane. Consequently, the excited-state configurations could have mixed *x*–*y* polarization. Such *x*–*y* mixing is reflected in a diminution in the S_2–S_1 angle θ_{12} from 90° and rotation of one or both of the TDM vectors off the traditional *x* and *y* axes (Fig. 7 and Table 2).

The S_1 and S_2 TDMs are orthogonal for **H-BC** and **BrNp-BC** (Fig. 7). The difference angle θ_{12} drops to 73° for **Es-BC** due to

substitution at only the 2,12 and not the 3,13 positions that flank the NH–HN (y) axis. This reduction in θ_{12} by 17° for **Es-BC** seems to imply significant x–y mixing. The extent of mixing is then progressively more substantial as θ_{12} decreases along the series **Phen-BC** (55°) > **Benz-BC** (46°) > **Phen^{2,1}-BC** (39°) (Fig. 7 and Table 2). Along the series of annulated bacteriochlorins, the $S_0 \rightarrow S_1$ intensity also drops dramatically (Fig. 2 and Table 2). In contrast, a relatively small amount of x–y mixing is implied by the electron distributions at the macrocycle positions for the MOs and NTOs of **Phen-BC**, **Benz-BC**, and **Phen^{2,1}-BC**, which are similar (but not identical) to those of **H-BC**, **Es-BC**, and **BrNp-BC** (Fig. 5 and 6).

Empirical x–y mixing model. These seemingly incongruous observations can be understood by considering a simple empirical x–y mixing model that assumes mixing of two transitions/states, one of which is purely y-polarized and the other is purely x-polarized. The focus here is mixing $S_0 \rightarrow S_1$ with $S_0 \rightarrow S_2$ because these transitions/states are the closest in energy and, for the annulated bacteriochlorins, their relative absorption intensities vary inversely (Fig. 2 and Table 2). **H-BC** and **BrNp-BC** provide reference points because the $S_0 \rightarrow S_1$ and $S_0 \rightarrow S_2$ transitions are perpendicular ($\theta_{12} \sim 90°$) and lie along the traditional y and x axes, respectively (Fig. 7). Mixing of x- and y-polarized transitions/states occurs for the other bacteriochlorins to varying extents. Under any mixing scenario (like the four-orbital model), a redistribution of transition dipole strength can occur between the two mixed transitions/states relative to the pure ones.

In the simple empirical model for understanding the observations, the transitions/states are mixed by a coefficient α, whose square is given in eqn (1) and plotted in Fig. 8. The function α^2 gives the amount of pure S_1 that remains in the new S_1 state upon mixing with pure S_2. Similarly, α^2 gives the amount of pure S_2 that remains in the new S_2 state upon mixing with pure S_1. Consider two limiting cases. When θ_{12} = 90°, α^2 = 1 and the new S_1 retains 100% of the original pure y-polarized S_1 character and the new S_2 retains 100% of the original pure x-polarized S_2 character, and both retain their original transition-dipole strengths. When θ_{12} = 0°, α^2 = 0.5, mixing is maximal, and the new S_1 and S_2 transitions/states both are 50/50 mixtures of the original pure x- and y-polarized transitions/states. In principle, all the transition-dipole strength could reside in one new transition and the other would be silent. However, the actual ratio would depend on the specific case and the intensity ratio with no x–y mixing (*e.g.*, that for **H-BC**).

$$\alpha^2 = [\cos(45° - |\theta_{12}|/2)]^2 \quad -90° \leq \theta_{12} \leq 90° \tag{1}$$

The above-noted quandary is solved by inspection of Fig. 8 for the specific cases (colored circles) for the various bacteriochlorins (Chart 1). For **Es-BC**, the TDM difference angle θ_{12} is 17° off orthogonal (Fig. 7(B)), yet α^2 = 0.98 and the S_1 state remains 98% the pure y-polarized S_1. For annulated **Phen^{2,1}-BC**, θ_{12} drops to 39° and the S_1 oscillator strength to f = 0.23 (Fig. 7 and Table 2), yet α^2 = 0.82 and the S_1 state remains 82% the pure y-polarized S_1. Thus, the electron distributions at the

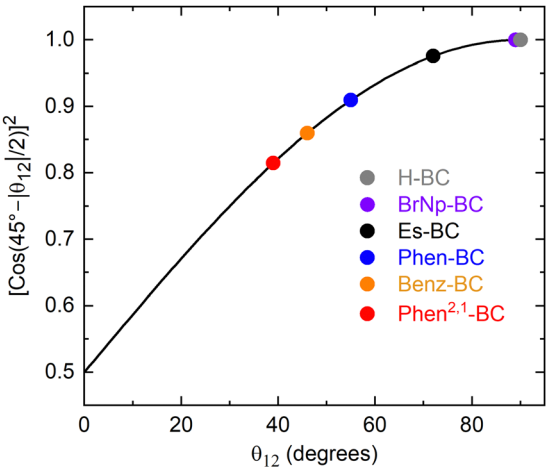

Fig. 8 Plot of the square of the mixing coefficient α as a function of the absolute value of the angle θ_{12} between the S_1 and S_2 TDM vectors.

macrocycle positions for the MOs and NTOs of **Phen^{2,1}-BC** are quite similar to those of **BrNp-BC**, **Es-BC**, and **H-BC** (Fig. 5 and 6). In short, it takes only a small amount of x–y mixing to substantially impact spectral and electronic properties such as the relative intensities of the $S_0 \rightarrow S_1$ and $S_0 \rightarrow S_2$ transitions and their directions in the molecular framework.

Effects of vibronic coupling. The vibrational progressions in the $S_0 \rightarrow S_1$ manifolds for **H-BC**, **Es-BC**, and **BrNp-BC** are typical of a bacteriochlorin with a strong $S_1(0,0)$ band and much weaker $S_1(1,0)$ and $S_1(2,0)$ features whose relative intensities are expected for a Franck–Condon progression for a large macrocyclic system (Fig. 2 and Table 2). The intensity profile for the $S_0 \rightarrow S_1$ manifold of **Phen-BC** is similar, but is now dominated by ~1300 cm^{-1} modes rather than a lower-energy accordion-like mode for the non-annulated analogues (*vide supra*). On the other hand, the optical properties of **Phen^{2,1}-BC** and **Benz-BC** show clear effects of Herzberg–Teller (vibronic) coupling[58–60] on the intensity distributions in the $S_0 \rightarrow S_1$ and $S_0 \rightarrow S_2$ manifolds (Fig. 2 and Table 2). The $S_1(1,0)$ bands of **Benz-BC** and **Phen^{2,1}-BC** and the $S_2(1,0)$ band of **Phen^{2,1}-BC** are all more intense than expected for a Franck–Condon progression (*vide supra*).

Vibronic mixing involving two transitions/states results in dipole strength shifting from one to the other. The extent of mixing between $S_0 \rightarrow S_1$ and $S_0 \rightarrow S_2$ transitions will increase the closer the two excited states are in energy. Thus, the mixing will be greater for annulated bacteriochlorins **Phen^{2,1}-BC** (~4580 cm^{-1}) and **Benz-BC** (~4250 cm^{-1}) than non-annulated analogues **H-BC** (~6440 cm^{-1}), **BrNp-BC** (~5930 cm^{-1}) and **Es-BC** (~5840 cm^{-1}) (Table 2). Key vibrations must also have the appropriate symmetry to mix the two transitions/states. The extent of electronic x–y mixing [indicated by θ_{12} between TDMs (Fig. 7 and Table 2)] and the extent of vibronic mixing [indicated intensity of the (1,0) absorption bands (Fig. 2)] increases along the series **Phen-BC** < **Benz-BC** < **Phen^{2,1}-BC**.

There is a parallel decrease in the S_1 excited-state lifetime along the same series (Table 2): **Phen-BC** (150 ps) > **Benz-BC**

(7 ps) > **Phen^{2,1}-BC** (0.4 ps). In all three cases, the S_1 decay is dominated by $S_1 \rightarrow S_0$ internal conversion, which is much more facile than expected based on the energy-gap law for non-radiative decay of normal bacteriochlorins (Fig. 4). The $S_1 \rightarrow S_0$ internal conversion process depends on the coupling of electronic and vibrational degrees of freedom, namely the breakdown of the Born–Oppenheimer approximation.[60–63] Thus, a reduction in symmetry links (1) the extent of electronic *x*–*y* mixing reflected in the angle between the $S_0 \rightarrow S_1$ and $S_0 \rightarrow S_2$ TDMs (Fig. 7), (2) the reduction in $S_0 \rightarrow S_1$ intensity (Fig. 2), (3) vibronic activity in the absorption spectra (Fig. 2), (4) an increased rate of internal conversion (Fig. 4), and (5) a diminished ring current measured by NMR spectroscopy (Table 1).

Outlook

The synthesis of **Phen^{2,1}-BC** described herein entailed development of a new route (Scheme 2) that is distinct from the prior route to annulated bacteriochlorins including **Benz-BC** and **Phen-BC** (Scheme 1), and may prove useful for construction of additional annulated bacteriochlorins. Annulation to form **Phen^{2,1}-BC**, **Benz-BC** and **Phen-BC** impacts electronic structure, optical properties, and excited-state dynamics in unexpected ways. The desired bathochromic shift of the $S_0 \rightarrow S_1$ transition into the NIR-II region is accompanied by diminished absorption strength and a shortened excited-state lifetime. These observables are connected to one another and to electronic *x*–*y* mixing and vibronic coupling involving the $S_0 \rightarrow S_1$ and $S_0 \rightarrow S_2$ transitions. The electronic and vibronic effects in turn arise from a reduction in symmetry entailed by the β-*meso* annulation motifs employed. The collective optical, excited-state, electronic and vibronic impacts of annulation were unexpected and have required analysis beyond the four-orbital model, which relies on symmetry partitioning of the relevant (orthogonal) *x*- and *y*-polarized electronic configurations.

The observations and calculations described herein reveal that the key heuristic in achieving strong $S_0 \rightarrow S_1$ absorption in the NIR-II region is to maintain *x*–*y* orthogonality. To this end, preliminary calculations on annulated bacteriochlorin **(Phen^{2,1})$_2$-BC** shown in Chart 2 give an angle between the $S_0 \rightarrow S_1$ and $S_0 \rightarrow S_2$ transition dipole moments of 82°, and an $S_0 \rightarrow S_1$ band at 1436 nm with a substantial oscillator strength of 0.33. It is anticipated that this architecture will also have an S_1 lifetime consistent with that predicted from bacteriochlorins that possess a high degree of *x*–*y* orthogonality. The synthesis and photophysical characterization of **(Phen^{2,1})$_2$-BC** and additional chromophores are required to assess the broad applicability of the picture that has emerged upon comparison of **Phen^{2,1}-BC** and other annulated bacteriochlorins described herein.

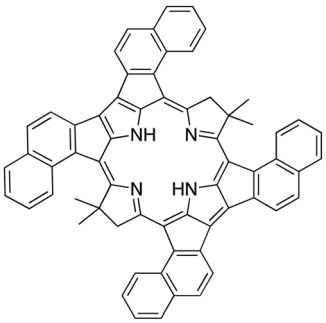

(Phen^{2,1})$_2$-BC

Chart 2 Fictive bacteriochlorin for deep NIR-II penetration.

Experimental section

Photophysical properties

Static absorption (Shimadzu UV-1800), static emission (Horiba Nanolog; PTI Quantamaster), and other measurements were performed at room temperature on dilute (μM), Ar-purged solutions of compounds in toluene. Some absorption spectra were acquired at 295 or 77 K on samples in 2-methyltetrahydrofuran. Determination of Φ_f values utilized samples with A ≤ 0.1 at the excitation wavelength and used *meso*-tetraphenylporphyrin in non-degassed toluene (Φ_f = 0.070)[45] or **Phen-BC** (Φ_f = 0.004)[21] as a standard. Transient absorption (TA) studies utilized an ultrafast laser system with (0.5–1 μJ) ~100 fs excitation flashes from a 1 kHz Ti:sapphire laser system (Spectra Physics) and Helios spectrometer (Ultrafast Systems). TA data were analyzed using Surface Xplorer (Ultrafast Systems), CarpetView (Light Conversion), and custom routines in OriginPro (OriginLab).

Density functional theory calculations

DFT calculations were performed with Gaussian 16 version C.01.[39] Calculations used the PCM model for the arrays in toluene. Molecular geometries were fully optimized using the hybrid B3LYP functional and the basis set 6-31G*. These calculations used Gaussian 16 defaults. Electron-density distributions and energies of the molecular orbitals (MOs) were obtained using the long-range corrected ωB97XD functional and the basis set 6-31++G**. TDDFT calculations were performed using the long-range corrected ωB97XD functional and the basis set 6-31++G** with the Gaussian 16 defaults and the additional keyword *n* states = 16. The MO, NTO, and TDM images were created in Chemcraft.

General synthetic methods

Tetrahydrofuran (THF) was freshly distilled from sodium/benzophenone ketyl. Silica (40 μm average particle size) was used for column chromatography. Other solvents (anhydrous or reagent-grade) were employed as received from commercial suppliers. ^{1}H NMR, ^{10}B NMR, and ^{13}C{^{1}H} NMR spectra were recorded at room temperature in $CDCl_3$ unless noted otherwise. Deactivated silica for chromatographic purification of acid-labile compounds was prepared by treatment with 3% triethylamine in hexanes followed by washing with hexanes. Deactivated silica for TLC analysis of acid-labile compounds was prepared by running with 3% triethylamine in hexanes followed by drying of the plate prior to the analysis. Electrospray ionization mass spectrometry (ESI-MS) data were obtained in the positive-ion mode (unless

noted otherwise) and are reported for the molecular ion or protonated molecular ion. Commercial compounds were used as received. The known compounds 1-bromo-2-(2-nitrovinyl)-naphthalene (**1**),[27] Michael acceptor **VII**,[33] and dihydrodipyrrin **I**[21] were prepared as described in the literature.

Synthetic procedures

(1-Bromonaphthalen-2-yl)boronic acid (V). The line drawing of the title compound has been displayed as the product of a reaction in a patent application[64] but to our knowledge without synthetic procedure and characterization data. Other papers (*e.g.*, ref. 65) report use of the title compound but again without synthesis or characterization data. Following a procedure,[66] a solution of isopropylmagnesium bromide (1.0 mL, 1.0 mmol, 2.0 M in THF) was added dropwise into a solution of 1-bromo-2-iodonaphthalene (333 mg, 1.00 mmol) in THF (0.505 M) at −78 °C. The resulting mixture was stirred at −78 °C for 1 h and the solution was then treated with trimethyl borate (104 mg, 2.30 mmol). The reaction mixture was allowed to warm to room temperature and further stirred for 1 h. The reaction mixture was acidified with hydrochloric acid (2 N, 1 : 1 volume HCl/volume THF) and stirred at room temperature for 2 h. The reaction mixture was diluted with water (10.0 mL) and extracted with ethyl acetate (3 × 15.0 mL). The combined organic extract was dried over anhydrous Na_2SO_4 and concentrated under reduced pressure. Column chromatography [silica, hexanes/ethyl acetate (5 : 1 to 7 : 3)] afforded a white solid (134.6 mg, 64%). m.p. 234–238 °C: ^{1}H NMR (600 MHz, CD_3OD) δ 8.22 (d, J = 8.46 Hz, 1H), 7.85–7.88 (m, 2H), 7.61 (t, 1H), 7.55 (t, 1H), 7.31 (d, J = 7.68 Hz, 1H); ^{13}C{^{1}H} NMR (150 MHz, CD_3OD) δ 136.2, 132.8, 129.4, 129.3, 128.8, 128.6, 128.1, 127.7, 126.3. The aromatic quaternary C–B(OH)$_2$ was not observed; ^{10}B NMR (54 MHz, $CDCl_3$) δ 29.6.

4-(1-Bromonaphthalen-2-yl)-3-ethoxycarbonyl-2-methylpyrrole (3). Following a procedure[25,26] with modification, samples of ethyl-3-aminobut-2-enoate (3.26 g, 25.3 mmol) and anhydrous $FeCl_3$ (547 mg, 3.37 mmol, 20.0 mol%) were added to a solution of 1-bromo-2-(2-nitrovinyl)naphthalene (4.69 g, 16.8 mmol) in toluene (168 mL). The reaction mixture was refluxed in a heated oil bath overnight with stirring. The reaction mixture was allowed to cool to room temperature and then diluted with ethyl acetate (50.0 mL). The resulting mixture was washed successively with 1 M HCl (100 mL), water (100 mL), and brine (100 mL). Each aqueous solution was extracted with ethyl acetate (2 × 80.0 mL). The combined organic extract was dried over anhydrous Na_2SO_4 and then concentrated under reduced pressure. Column chromatography [silica, hexanes/ethyl acetate (9 : 1 to 4 : 1)] afforded a light-yellow solid (2.86 g, 47%). m.p. 175–176 °C; ^{1}H NMR (500 MHz, $CDCl_3$) δ 8.42 (br, 1H), 8.36 (d, J = 8.6 Hz, 1H), 7.83 (d, J = 8.2 Hz, 1H), 7.76 (d, J = 8.3 Hz, 1H), 7.55–7.60 (m, 1H), 7.47–7.51 (m, 1H), 7.40 (d, J = 8.4 Hz, 1H), 6.58 (d, J = 2.4 Hz, 1H), 4.00 (q, J = 7.2 Hz, 2H), 2.58 (s, 3H), 0.83 (t, J = 7.1 Hz, 3H); ^{13}C{^{1}H} NMR (125 MHz, $CDCl_3$) δ 165.5, 135.9, 135.4, 133.4, 132.3, 129.6, 128.0, 127.7, 127.2, 126.6, 126.4, 126.0, 124.6, 115.9, 111.3, 59.2, 13.8, 13.7; ESI-MS obsd 358.0434, calcd 358.0437 [(M + H)$^+$, M = $C_{18}H_{16}BrNO_2$].

4-(1-Bromonaphthalen-2-yl)-3-ethoxycarbonyl-2-formylpyrrole (4). Following a procedure,[29] NaH 60% dispersion in mineral oil (670 mg, 17 mmol) was added into a solution of **3** (3.32 g, 9.30 mmol) in THF (62.0 mL) at 0 °C (ice bath). The reaction mixture was stirred at 0 °C for 30 min. Triisopropylsilyl chloride (2.32 g, 12.0 mmol) was added in one portion to the reaction mixture at 0 °C. The resulting mixture was stirred at 0 °C for 30 min. The reaction mixture was washed with water (100 mL) and brine (100 mL). Each aqueous solution was extracted with ethyl acetate (2 × 100 mL). The combined organic extract was dried over anhydrous Na_2SO_4 and then concentrated under reduced pressure. Samples of THF (31.0 mL), glacial acetic acid (31.0 mL), and water (31.0 mL) were added successively to the crude mixture. The resulting mixture was cooled to 0 °C. Cerium ammonium nitrate (20.3 g, 37.2 mmol) was added in one portion to the reaction mixture at 0 °C. The resulting mixture was stirred at 0 °C for 15 min and then diluted with ethyl acetate (100 mL). The mixture was washed with water (100 mL), saturated $NaHCO_3$ (150 mL), and brine (150 mL). Each aqueous solution was extracted with ethyl acetate (2 × 100 mL). The combined organic extract was dried over anhydrous Na_2SO_4 and then concentrated under reduced pressure. Column chromatography [silica, hexanes/ethyl acetate (9 : 1 to 5 : 1)] afforded an orange solid (1.88 g, 54%). m.p. 196–197 °C; ^{1}H NMR (600 MHz, $CDCl_3$) δ 10.29 (d, J = 0.7 Hz, 1H), 10.20 (br, 1H), 8.35 (d, J = 8.5 Hz, 1H), 7.86 (d, J = 8.0 Hz, 1H), 7.81 (d, J = 8.3 Hz, 1H), 7.59–7.63 (m, 1H), 7.52–7.56 (m, 1H), 7.40 (d, J = 8.3 Hz, 1H), 7.10 (dd, J = 2.9, 0.6 Hz, 1H), 4.13 (q, J = 7.2 Hz, 2H), 0.94 (t, J = 7.1 Hz, 3H); ^{13}C{^{1}H} NMR (150 MHz, $CDCl_3$) δ 182.3, 163.4, 133.8, 133.4, 133.1, 132.3, 129.2, 128.8, 128.1, 127.8, 127.6, 126.9, 126.6, 124.7, 124.4, 121.2, 60.6, 13.7; ESI-MS obsd 372.0229, calcd 372.0230 [(M + H)$^+$, M = $C_{18}H_{14}BrNO_3$].

4-(1-Bromonaphthalen-2-yl)-3-ethoxycarbonyl-2-(2-nitroethyl) pyrrole (5). Following a procedure,[29] nitromethane (3.55 g, 58.1 mmol) was added to a mixture of **4** (2.40 g, 6.46 mmol), KOAc (634 mg, 6.46 mmol), and CH_3NH_2·HCl (436 mg, 6.46 mmol) in THF (52.0 mL) and ethanol (13.0 mL). The reaction mixture was stirred at room temperature for 10 h. The reaction mixture was diluted with ethyl acetate (50.0 mL) and then washed with water (100 mL) and brine (100 mL). Each aqueous solution was extracted with ethyl acetate (2 × 100 mL). The combined organic extract was dried over anhydrous Na_2SO_4 and then concentrated under reduced pressure. The crude product was treated successively with chloroform (48.0 mL), isopropyl alcohol (16.0 mL), and silica (58 g). The mixture was stirred at room temperature for 30 min, and then $NaBH_4$ (488 mg, 12.9 mmol) was added. The reaction mixture was stirred at room temperature for 3 h. The resulting mixture was filtered and washed with water (100 mL) and brine (100 mL). Each aqueous solution was extracted with ethyl acetate (3 × 100 mL). The combined organic extract was dried over anhydrous Na_2SO_4 and then concentrated under reduced pressure. Column chromatography [silica, hexanes/dichloromethane (1 : 4 to 1 : 9)] afforded a light-yellow solid (1.20 g, 45%). m.p. 129–130 °C; ^{1}H-NMR (500 MHz, $CDCl_3$) δ 8.62 (br, 1H), 8.35 (d, J = 8.4 Hz, 1H), 7.85 (d, J = 8.1 Hz, 1H), 7.77 (d, J = 8.3 Hz, 1H), 7.57–

7.62 (m, 1H), 7.49–7.54 (m, 1H), 7.38 (d, J = 8.4 Hz, 1H), 6.69 (d, J = 2.6 Hz, 1H), 4.78–4.83 (m, 2H), 3.97 (q, J = 7.0 Hz, 2H), 3.63–3.69 (m, 2H), 0.75 (t, J = 7.2 Hz, 3H); $^{13}C\{^1H\}$ NMR (125 MHz, $CDCl_3$) δ 165.1, 135.2, 133.4, 133.2, 132.2, 129.3, 128.0, 127.7, 127.3, 126.7, 126.5, 126.2, 124.8, 117.3, 112.1, 74.6, 59.6, 25.4, 13.6; ESI-MS obsd 417.0441, calcd 417.0444 [$(M + H)^+$, M = $C_{19}H_{17}BrN_2O_4$].

4-(1-Bromonaphthalen-2-yl)-3-ethoxycarbonyl-2-(6,6-dimethoxy-3,3-dimethoxy-2-nitro-5-oxohexyl)pyrrole (6). Following a procedure,[29,34] a sample of **5** (226 mg, 0.543 mmol) was dissolved in THF (2.0 mL) and concentrated to a minimum volume under reduced pressure. Michael acceptor **VII** (257 mg, 1.63 mmol) and 1,8-diazabicyclo(5.4.0)undec-7-ene (248 mg, 1.63 mmol) were then added. The reaction mixture was stirred at room temperature for 18 h. The reaction mixture was diluted with ethyl acetate (20.0 mL) and washed with saturated NH_4Cl (20.0 mL) and brine (20.0 mL). Each aqueous solution was extracted with ethyl acetate (2 × 20.0 mL). The combined organic extract was dried over anhydrous Na_2SO_4 and then concentrated under reduced pressure. Column chromatography [silica, hexanes/ethyl acetate (6 : 1)] afforded a light-yellow solid (224 mg, 72%). m.p. 48–51 °C; ^1H NMR (500 MHz, $CDCl_3$) δ 8.45 (br, 1H), 8.33 (d, J = 8.6 Hz, 1H), 7.83 (d, J = 8.2 Hz, 1H), 7.75 (d, J = 8.4 Hz, 1H), 7.55–7.60 (m, 1H), 7.47–7.52 (m, 1H), 7.36 (d, J = 8.2 Hz, 1H), 6.61 (d, J = 2.6 Hz, 1H), 5.28 (ABX, $^3J_{AX}$ = 11.8 Hz, $^3J_{BX}$ = 2.3 Hz, 1H), 4.43 (s, 1H), 3.91–4.04 (m, 2H), 3.85 (ABX, $^2J_{AB}$ = 14.6 Hz, $^3J_{BX}$ = 2.4 Hz, 1H), 3.44 (s, 3H), 3.43 (s, 3H), 3.38 (ABX, $^2J_{AB}$ = 14.4 Hz, $^3J_{AX}$ = 11.8 Hz, 1H), 2.76, 2.69 (AB, ^2J = 18.6 Hz, 2H), 1.34 (s, 3H), 1.22 (s, 3H), 0.74 (t, J = 7.1 Hz, 3H); $^{13}C\{^1H\}$ NMR (125 MHz, $CDCl_3$) δ 203.2, 164.8, 135.5, 133.4, 133.0, 132.2, 129.4, 128.0, 127.7, 127.2, 126.7, 126.4, 126.1, 124.8, 117.3, 112.2, 104.5, 94.8, 59.4, 54.99, 54.97, 44.7, 36.7, 26.6, 24.1, 23.7, 13.6; ESI-MS obsd 575.1381, calcd 575.1387 [$(M + H)^+$, M = $C_{27}H_{31}BrN_2O_7$].

8-(1-Bromonaphthalen-2-yl)-7-ethoxycarbonyl-1-(1,1-dimethoxymethyl)-2,2-dimethyl-2,3-dihydrodipyrrin (7). Following a procedure[29,34] with modifications, in a first flask, a solution of **6** (553 mg, 0.961 mmol) and potassium *tert*-butoxide (153 mg, 1.25 mmol) in THF (9.6 mL) was degassed by bubbling with argon at room temperature for 45 min. In a second flask, a mixture of $TiCl_3$ (10–15% in 12% HCl solution, 9.9 mL, 7.7 mmol), NH_4OAc (29.6 g, 384 mmol), and water (43.0 mL) was degassed by bubbling with argon at room temperature for 45 min. The solution in the second flask was transferred into the solution in the first flask. The resulting mixture was stirred in an oil bath at 40 °C for 20 h. The reaction mixture was diluted with ethyl acetate (100 mL). The organic mixture was washed with water (100 mL), saturated $NaHCO_3$ (100 mL), and brine (100 mL). Each aqueous solution was extracted with ethyl acetate (2 × 100 mL). The combined organic extract was dried over anhydrous Na_2SO_4 and then concentrated under reduced pressure. Column chromatography [silica, hexanes/ethyl acetate (14 : 1 to 9 : 1)] afforded a light-yellow solid (228 mg, 44%). m.p. 161–162 °C; ^1H NMR (600 MHz, $CDCl_3$) δ 11.35 (br, 1H), 8.36 (d, J = 8.5 Hz, 1H), 7.84 (d, J = 8.2 Hz, 1H), 7.76 (d, J = 8.3 Hz, 1H), 7.56–7.60 (m, 1H), 7.48–7.52 (m, 1H), 7.42 (d, J = 8.2 Hz, 1H), 6.97 (s, 1H), 6.81 (d, J = 2.5 Hz, 1H), 5.06 (s, 1H), 4.00 (q, J = 7.1 Hz, 2H), 3.48 (s, 6H), 2.68 (s, 2H), 1.29 (s, 6H), 0.78 (t, J = 1.1 Hz, 3H); $^{13}C\{^1H\}$ (125 MHz, $CDCl_3$) δ 177.1, 165.3, 164.1, 136.1, 135.3, 133.4, 132.3, 129.6, 128.0, 127.7, 127.1, 126.5, 126.4, 126.0, 124.7, 118.9, 111.6, 105.9, 102.5, 59.2, 54.6, 48.3, 40.6, 29.0; ESI-MS obsd 525.1382, calcd 525.1384 [$(M + H)^+$, M = $C_{27}H_{29}BrN_2O_4$].

3,13-Bis(1-bromonaphthalen-2-yl)-2,12-bis(ethoxycarbonyl)-8,8,18,18-tetramethylbacteriochlorin (BrNp-BC). Following a procedure,[29] $BF_3{\cdot}OEt_2$ (305 mg, 255 μL, 2.15 mmol) was added to a solution of **7** (308 mg, 0.586 mmol) in anhydrous dichloromethane (36.6 mL) under argon atmosphere. The reaction mixture was stirred at room temperature for 28 h. The reaction mixture was diluted with dichloromethane (20.0 mL) and then washed with saturated aqueous $NaHCO_3$ (50.0 mL) and brine (50.0 mL). Each aqueous solution was extracted with ethyl acetate (2 × 50.0 mL). The combined organic extract was dried over anhydrous Na_2SO_4 and then concentrated under reduced pressure. Column chromatography [deactivated silica, hexanes/ethyl acetate (6 : 1)] afforded a dark-purple solid (34.4 mg, 12%). ^1H NMR (600 MHz, $CDCl_3$) δ 9.75 (br, 2H), 8.55 (d, J = 8.2 Hz, 2H), 8.29 (s, 2H), 8.07–8.13 (m, 4H), 7.86 (t, J = 8.4 Hz, 2H), 7.77 (t, J = 7.9 Hz, 2H), 7.72 (t, J = 7.5 Hz, 2H), 4.41–4.48 (m, 2H), 4.32–4.39 (m, 2H), 4.18–4.23 (m, 4H), 1.89–1.90 (m, 12H), 1.02 (t, J = 7.1 Hz, 6H), −1.05 (s, 2H); $^{13}C\{^1H\}$ NMR (150 MHz, $CDCl_3$) δ 173.6, 165.5, 160.5, 138.51, 138.47, 135.8, 135.6, 134.1, 132.8, 132.40, 132.38, 129.9, 129.8, 128.41, 128.39, 127.90, 127.88, 127.84, 126.9, 126.72, 126.70, 125.68, 125.65, 120.41, 120.3, 99.4, 97.6, 60.6, 51.2, 46.2, 31.2, 31.0, 30.9, 30.8, 13.8; ESI-MS obsd 925.1763, calcd 925.1782 [$(M + H)^+$, M = $C_{50}H_{44}Br_2N_4O_4$]. λ_{abs} (toluene) 384, 359, 529, 771 nm. No evidence (by TLC analysis or ^1H NMR spectroscopy) was observed for the presence of atropisomers. On the other hand, $^{13}C\{^1H\}$ NMR analysis showed 35 signals whereas 25 were expected, which is attributed to the presence of atropisomers. Similar observations were made for the analogous precursors to **Phen-BC** and **Benz-BC**.[21]

Phen^{2,1}-BC

Following a procedure,[21] a mixture of **BrNp-BC** (34.3 mg, 37.2 μmol), $PCy_3{\cdot}HBF_4$ (41.0 mg, 111 μmol), and K_2CO_3 (25.6 mg, 185 μmol) in anhydrous DMF (3.7 mL) in a Schlenk flask was freeze-pumped-thawed for 3 cycles. $Pd(OAc)_2$ (8.33 mg, 37.1 μmol) was added into the mixture, which was then heated in an oil bath at 110 °C for 2 h. The reaction mixture was allowed to cool to room temperature and then was diluted with dichloromethane (10.0 mL). The resulting mixture was washed with water (15.0 mL) and brine (15.0 mL). Each aqueous solution was extracted with ethyl acetate (2 × 15.0 mL). The combined organic extract was dried over anhydrous Na_2SO_4 and then concentrated under reduced pressure. The crude mixture was passed through a deactivated silica pad, eluted with ethyl acetate, and concentrated under reduced pressure. Preparative thin-layer chromatography [deactivated silica, hexanes/ethyl acetate (4 : 1)] afforded a dark-brown solid (4.5 mg, 16%). ^1H NMR (600 MHz, $CDCl_3$) δ 8.03 (d, J = 8.0 Hz, 2H), 7.95 (d, J = 8.5 Hz, 2H), 7.77 (s, 2H), 7.62 (d, J = 8.1 Hz, 2H), 7.43

(t, J = 7.6 Hz, 2H), 7.37 (d, J = 8.2 Hz, 2H), 7.43 (t, J = 7.3 Hz, 2H), 4.43 (q, J = 7.1 Hz, 4H), 3.49 (s, 4H), 3.21 (s, 2H), 1.49 (t, J = 7.0, 6H), 1.20 (s, 12H); $^{13}C\{^1H\}$ NMR (150 MHz, $CDCl_3$) δ 174.2, 164.5, 159.2, 146.0, 143.7, 143.6, 142.2, 135.9, 134.7, 129.7, 129.2, 127.7, 125.6, 125.45, 125.40, 123.7, 117.9, 112.2, 101.1, 60.7, 52.3, 46.2, 28.3, 14.5; ESI-MS obsd 762.3184, calcd 762.3200 [$(M + H)^+$, M = $C_{50}H_{42}N_4O_4$]. λ_{abs} (toluene) 374, 401, 455, 750, 1110, 1292 nm.

Molar absorption coefficients

The molar absorption coefficients were determined by preparing 0.20 mM **Phen^{2,1}-BC** (0.97 mg) in toluene (6.6 mL) and **BrNp-BC** (0.98 mg) in toluene (5.3 mL). Known volumes of the mother solution (120, 180, 240, 300, and 360 μL for **Phen^{2,1}-BC** and 20, 30, 40, 50, and 60 μL for **BrNp-BC**) were diluted with toluene to 3.0 mL for instrumental measurement. The absorption spectra were recorded at room temperature. The averages of three runs were calculated: **BrNp-BC** ($\varepsilon_{384\,nm}$ = 64 500 M^{-1} cm^{-1}; $\varepsilon_{359\,nm}$ = 100 600 M^{-1} cm^{-1}; $\varepsilon_{529\,nm}$ = 25 100 M^{-1} cm^{-1}; and $\varepsilon_{771\,nm}$ = 125 900 M^{-1} cm^{-1}); **Phen^{2,1}-BC** ($\varepsilon_{347\,nm}$ = 32 400 M^{-1} cm^{-1}; $\varepsilon_{401\,nm}$ = 33 200 M^{-1} cm^{-1}; $\varepsilon_{455\,nm}$ = 39 500 M^{-1} cm^{-1}; $\varepsilon_{750\,nm}$ = 19 000 M^{-1} cm^{-1}; $\varepsilon_{1110\,nm}$ = 6000 M^{-1} cm^{-1}; and $\varepsilon_{1292\,nm}$ = 6100 M^{-1} cm^{-1}).

Single-crystal X-ray diffraction analyses

SCXRD data were obtained using a Bruker D8 Venture diffractometer at 100 K (MoKα = 0.71073 Å). The structural refinement and graphics were calculated and generated using APEX4, SHELXL, OLEX2, and MERCURY3 software.

Conflicts of interest

There are no conflicts of interest to declare.

Acknowledgements

This work was supported by a grant from the Chemical Sciences, Geosciences and Biosciences Division, Office of Basic Energy Sciences, of the U.S. Department of Energy (DE-FG02-05ER15661), and by NC State University. Compound characterization was performed in part by the Molecular Education, Technology and Research Innovation Center (METRIC) at NC State University, which is supported by the State of North Carolina. XRD analyses were performed at University of Tennessee at Knoxville.

References

1 A. M. Smith, M. C. Mancini and S. Nie, *Nat. Nanotechnol.*, 2009, **4**, 710–711.
2 D. Meng, R. Zheng, Y. Zhao, E. Zhang, L. Dou and Y. Yang, *Adv. Mater.*, 2022, **34**, 2107330.
3 C. Han, B. K. Kundu, Y. Liang and Y. Sun, *Adv. Mater.*, 2024, **36**, 2307759.
4 S. Zhu, R. Tian, A. L. Antaris, X. Chen and H. Dai, *Adv. Mater.*, 2019, **31**, 1900321.
5 Z. Guo, S. Park, J. Yoon and I. Shin, *Chem. Soc. Rev.*, 2014, **43**, 16–29.
6 N.-N. Zhang, C.-Y. Lu, M.-J. Chen, X.-L. Xu, G.-F. Shu, Y.-Z. Du and J.-S. Ji, *J. Nanobiotechnol.*, 2021, **19**, 132.
7 H. Li, Y. Kim, H. Jung, J. Y. Hyun and I. Shin, *Chem. Soc. Rev.*, 2022, **51**, 8957–9008.
8 X. Liu, B. Yu, Y. Shen and H. Cong, *Coord. Chem. Rev.*, 2022, **468**, 214609.
9 B. Dunn, M. Hanafi, J. Hummel, J. R. Cressman, R. Veneziano and P. V. Chitnis, *Bioengineering*, 2023, **10**, 954.
10 M. Taniguchi and J. S. Lindsey, *Photochem. Photobiol.*, 2021, **97**, 136–165.
11 M. Kobayashi, M. Akiyama, H. Kise and T. Watanabe, in *Chlorophylls and Bacteriochlorophylls: Biochemistry, Biophysics, Functions and Applications*, ed. B. Grimm, R. J. Porra, W. Rüdiger and H. Scheer, Springer, Dordrecht, The Netherlands, 2006, pp. 55–66.
12 H. Scheer, in *Chlorophylls and Bacteriochlorophylls. Biochemistry, Biophysics, Functions and Application*, ed. B. Grimm, R. J. Porra, W. Rüdiger and H. Scheer, Springer, Dordrecht, The Netherlands, 2006, pp. 1–26.
13 M. Kobayashi, S. Akutsu, D. Fujinuma, H. Furukawa, H. Komatsu, Y. Hotota, Y. Kato, Y. Kuroiwa, T. Watanabe, M. Ohnishi-Kameyama, H. Ono, S. Ohkubo and H. Miyashita, in *Photosynthesis*, ed. Z. Dubinsky, 2013, pp. 47–90.
14 J. W. Springer, K. M. Faries, J. R. Diers, C. Muthiah, O. Mass, H. L. Kee, C. Kirmaier, J. S. Lindsey, D. F. Bocian and D. Holten, *Photochem. Photobiol.*, 2012, **88**, 651–674.
15 A. Maccoll, *Q. Rev.*, 1947, **1**, 16–58.
16 L. N. Ferguson, *Chem. Rev.*, 1948, **43**, 385–446.
17 K. Venkataraman, *The Chemistry of Synthetic Dyes*, Academic Press, New York, 1952, vol. I, pp. 323–400.
18 S. Dähne, *Science*, 1978, **199**, 1163–1167.
19 M. Gouterman, *The Porphyrins*, ed. D. Dolphin, Academic Press, New York, 1978, vol. 3, pp. 1–165.
20 P. Vairaprakash, E. Yang, T. Sahin, M. Taniguchi, M. Krayer, J. R. Diers, A. Wang, D. M. Niedzwiedzki, C. Kirmaier, J. S. Lindsey, D. F. Bocian and D. Holten, *J. Phys. Chem. B*, 2015, **119**, 4382–4395.
21 H. Fujita, H. Jing, M. Krayer, S. Allu, G. Veeraraghavaiah, Z. Wu, J. Jiang, J. R. Diers, N. C. M. Magdaong, A. K. Mandal, A. Roy, D. M. Niedzwiedzki, C. Kirmaier, D. F. Bocian, D. Holten and J. S. Lindsey, *New J. Chem.*, 2019, **43**, 7209–7232.
22 V.-P. Tran, P. Wang, N. Matsumoto, S. Liu, H. Jing, P. Nalaoh, K. Chau Nguyen, M. Taniguchi and J. S. Lindsey, *J. Porphyrins Phthalocyanines*, 2023, **27**, 1502–1551.
23 R. Martin and S. L. Buchwald, *Acc. Chem. Res.*, 2008, **41**, 1461–1473.
24 I. P. Beletskaya and A. V. Cheprakov, *Chem. Rev.*, 2000, **100**, 3009–3066.

25 S. Maiti, S. Biswas and U. Jana, *J. Org. Chem.*, 2010, **75**, 1674–1683.
26 L. Li, M.-N. Zhao, Z.-H. Ren, J. Li and Z.-H. Guan, *Synthesis*, 2012, 532–549.
27 A. Kolarovic, A. Käslin and H. Wennemers, *Org. Lett.*, 2014, **16**, 4236–4239.
28 D. Akbaslar, E. S. Giray and O. Algul, *Mol. Diversity*, 2021, **25**, 2321–2338.
29 H. Jing, P. Wang, B. Chen, J. Jiang, P. Vairaprakash, S. Liu, J. Rong, C.-Y. Chen, P. Nalaoh and J. S. Lindsey, *New J. Chem.*, 2022, **46**, 5534–5555.
30 M. Gałęzowski and D. T. Gryko, *J. Org. Chem.*, 2006, **71**, 5942–5950.
31 F. A. Luzzio, *Tetrahedron*, 2001, **57**, 915–945.
32 T. Tokoroyama, *Eur. J. Org. Chem.*, 2010, 2009–2016.
33 O. Mass and J. S. Lindsey, *J. Org. Chem.*, 2011, **76**, 9478–9487.
34 D. T. M. Chung, P. V. Tran, K. Chau Nguyen, P. Wang and J. S. Lindsey, *New J. Chem.*, 2021, **45**, 13302–13316.
35 J. E. McMurry and J. Melton, *J. Org. Chem.*, 1973, **38**, 4367–4373.
36 V.-P. Tran, N. Matsumoto, P. Nalaoh, H. Jing, C.-Y. Chen and J. S. Lindsey, *Organics*, 2022, **3**, 262–274.
37 C.-Y. Chen, M. Taniguchi and J. S. Lindsey, *J. Porphyrins Phthalocyanines*, 2014, **18**, 433–456.
38 M. Krayer, M. Ptaszek, H.-J. Kim, K. R. Meneely, D. Fan, K. Secor and J. S. Lindsey, *J. Org. Chem.*, 2010, **75**, 1016–1039.
39 M. J. Frisch, G. W. Trucks, H. B. Schlegel, G. E. Scuseria, M. A. Robb, J. R. Cheeseman, G. Scalmani, V. Barone, G. A. Petersson, H. Nakatsuji, X. Li, M. Caricato, A. V. Marenich, J. Bloino, B. G. Janesko, R. Gomperts, B. Mennucci, H. P. Hratchian, J. V. Ortiz, A. F. Izmaylov, J. L. Sonnenberg, D. Williams-Young, F. Ding, F. Lipparini, F. Egidi, J. Goings, B. Peng, A. Petrone, T. Henderson, D. Ranasinghe, V. G. Zakrzewski, J. Gao, N. Rega, G. Zheng, W. Liang, M. Hada, M. Ehara, K. Toyota, R. Fukuda, J. Hasegawa, M. Ishida, T. Nakajima, Y. Honda, O. Kitao, H. Nakai, T. Vreven, K. Throssell, J. A. Montgomery, Jr., J. E. Peralta, F. Ogliaro, M. J. Bearpark, J. J. Heyd, E. N. Brothers, K. N. Kudin, V. N. Staroverov, T. A. Keith, R. Kobayashi, J. Normand, K. Raghavachari, A. P. Rendell, J. C. Burant, S. S. Iyengar, J. Tomasi, M. Cossi, J. M. Millam, M. Klene, C. Adamo, R. Cammi, J. W. Ochterski, R. L. Martin, K. Morokuma, O. Farkas, J. B. Foresman and D. J. Fox, Gaussian, Inc., Wallingford CT, 2019.
40 M. Gouterman, *J. Chem. Phys.*, 1959, **30**, 1139–1161.
41 M. Gouterman, *J. Mol. Spectrosc.*, 1961, **6**, 138–163.
42 Y. Liu, S. Allu, M. N. Reddy, D. Hood, J. R. Diers, D. F. Bocian, D. Holten and J. S. Lindsey, *New J. Chem.*, 2017, **41**, 4360–4376.
43 E. Yang, C. Kirmaier, M. Krayer, M. Taniguchi, H.-J. Kim, J. R. Diers, D. F. Bocian, J. S. Lindsey and D. Holten, *J. Phys. Chem. B*, 2011, **115**, 10801–10816.
44 J. R. Diers, Q. Tang, C. J. Hondros, C.-Y. Chen, D. Holten, J. S. Lindsey and D. F. Bocian, *J. Phys. Chem. B*, 2014, **118**, 7520–7532.
45 M. Taniguchi, J. S. Lindsey, D. F. Bocian and D. Holten, *J. Photochem. Photobiol., C*, 2021, **46**, 100401.
46 W. Wild, A. Seilmeier, N. H. Gottfried and W. Kaiser, *Chem. Phys. Lett.*, 1985, **119**, 259–263.
47 E. R. Henry, W. A. Eaton and R. M. Hochstrasser, *Proc. Natl. Acad. Sci. U. S. A.*, 1986, **83**, 8982–8986.
48 J. R. Hill and D. D. Dlott, *J. Chem. Phys.*, 1988, **89**, 842–858.
49 T.-C. Chang and D. D. Dlott, *J. Chem. Phys.*, 1989, **90**, 3590–3602.
50 F. Laermer, T. Elsaesser and W. Kaiser, *Chem. Phys. Lett.*, 1989, **156**, 381–386.
51 A. Mokhtari, J. Chesnoy and A. Laubereau, *Chem. Phys. Lett.*, 1989, **155**, 593–598.
52 G. Angel, R. Gagel and A. Laubereau, *Chem. Phys.*, 1989, **131**, 129–134.
53 U. Sukowski, A. Seilmeier, T. Elsaesser and S. F. Fischer, *J. Chem. Phys.*, 1990, **93**, 4094–4101.
54 J. Rodriguez, C. Kirmaier and D. Holten, *J. Chem. Phys.*, 1991, **94**, 6020–6029.
55 O. Bilsel, S. N. Milam, G. S. Girolami, K. S. Suslick and D. Holten, *J. Phys. Chem.*, 1993, **97**, 7216–7221.
56 R. L. Martin, *J. Chem. Phys.*, 2003, **118**, 4775–4777.
57 A. K. Mandal, M. Taniguchi, J. R. Diers, D. M. Niedzwiedzki, C. Kirmaier, J. S. Lindsey, D. F. Bocian and D. Holten, *J. Phys. Chem. A*, 2016, **120**, 9719–9731.
58 G. Herzberg and E. Teller, *Z. Physikal. Chem. B*, 1933, **21**, 410–446.
59 M. H. Perrin, M. Gouterman and C. L. Perrin, *J. Chem. Phys.*, 1969, **50**, 4137–4150.
60 J. B. Birks, *Photophysics of Aromatic Molecules*, Wiley-Interscience, London, 1970, pp. 142–192.
61 G. W. Robinson and R. P. Frosch, *J. Chem. Phys.*, 1962, **37**, 1962–1973.
62 W. Siebrand, *J. Chem. Phys.*, 1967, **46**, 440–447.
63 R. Englman and J. Jortner, *Mol. Phys.*, 1970, **18**, 145–164.
64 H. Cai and C. Han, CN107698486, 2018.
65 L. Ling, Z. Song, H. Shan, C. Wang, S. Li, Y. Wang, J. Hu, Q. Chen, H. Zhang and Y. Yang, *Chem. Commun.*, 2023, **59**, 2739–2742.
66 M. Lanzi, Q. Dherbassy and J. Wencel-Delord, *Angew. Chem., Int. Ed.*, 2021, **60**, 14852–14857.